QUENCHING AND ROTATIONAL ENERGY TRANSFER IN MOLECULAR BROMINE: Br_2 $B^3\Pi(O_u^+)$

THESIS

Dean A. Massman
Captain, US Army

AFIT/GEP/ENP/91-J

DEPARTMENT OF THE AIR FORCE
AIR UNIVERSITY
AIR FORCE INSTITUTE OF TECHNOLOGY

Wright-Patterson Air Force Base, Ohio

AFIT/GEP/ENP/91-J

QUENCHING AND ROTATIONAL ENERGY TRANSFER IN MOLECULAR BROMINE: Br_2 $B^3\Pi(O_u^+)$

THESIS

Dean A. Massman
Captain, US Army

AFIT/GEP/ENP/91-J

Approved for public release; distribution unlimited

REPORT DOCUMENTATION PAGE

Form Approved
OMB No 0704-0188

1. AGENCY USE ONLY (Leave blank)	2. REPORT DATE	3. REPORT TYPE AND DATES COVERED
	May 1991	Master's Thesis

4. TITLE AND SUBTITLE

Quenching and Rotational Energy Transfer in Molecular Bromine: Br2(B)

5. FUNDING NUMBERS

6. AUTHOR(S)

Dean A. Massman, Captain, U. S. Army

7. PERFORMING ORGANIZATION NAME(S) AND ADDRESS(ES)

Air Force Institute of Technology
WPAFB, OH 45433-6583

8. PERFORMING ORGANIZATION REPORT NUMBER

AFIT/GEP/ENP/91J-1

9. SPONSORING MONITORING AGENCY NAME(S) AND ADDRESS(ES)

10. SPONSORING MONITORING AGENCY REPORT NUMBER

11. SUPPLEMENTARY NOTES

12a. DISTRIBUTION AVAILABILITY STATEMENT

Approved For Public Release; Distribution Unlimited

12b. DISTRIBUTION CODE

13. ABSTRACT (Maximum 200 words)

This study investigates the rotational energy transfer processes of optically excited bromine molecules in the presence of several collision partners. Resolved laser induced fluorescence spectra of collisionally populated rotational states were analyzed by means of Stern-Volmer analysis. Total rotational removal rate coefficients and state-to-state rotational removal rate coefficients for the v'=11,J'=35 level of Br2(B) were obtained for collisions with Br2(X), He, Ar and Xe. Rotational removal rate coefficients were also obtained for the v'=11, J'=26 and 47; v'=14, J'=36 states of Br2(B) with collisions with Ar. Total rotational removal rate for Br2 self quenching found to be 3.98+/-0.2x10-10 (cm3/Molec-Sec). Rate coefficients were scaled with respect to reduced mass of collision system and in accordance with exponential energy gap scaling law. Energy gap scaling law fit data well. Rotational removal rates displayed behavior to increase with increase in v' and J' of optically excited parent state. Possible J dependence displayed in results.

14. SUBJECT TERMS	15. NUMBER OF PAGES
Diatomic Bromine, Kinetics, Electronic Quenching, Rotational Energy Transfer, Halogen Spectroscopy, Laser Excitation	104
	16. PRICE CODE

17. SECURITY CLASSIFICATION OF REPORT	18. SECURITY CLASSIFICATION OF THIS PAGE	19. SECURITY CLASSIFICATION OF ABSTRACT	20. LIMITATION OF ABSTRACT
Unclassified	Unclassified	Unclassified	UL

AFIT/GEP/ENP/91-J

QUENCHING AND ROTATIONAL ENERGY TRANSFER IN MOLECULAR BROMINE: Br_2 $B^3\Pi(O_u^+)$

THESIS

Presented to the Faculty of the School of Engineering
of the Air Force Institute of Technology
Air University
In Partial Fulfillment of the
Requirements for the Degree of
Master of Science in Engineering Physics

Dean A. Massman
Captain, US Army

May 1991

PREFACE

The purpose of this research was to analyze rotational energy transfer processes in optically excited bromine gas with the goal of extracting rotational energy transfer rates and identifying appropriate scaling laws that fit these results. Though Diatomic Bromine is a poor candidate for a short wave visible chemical laser due to a high rate of predissociation, rotational energy transfer studies in general are important in analyzing potential SWVCL lasant species.

Resolved and unresolved emission spectra of optically excited bromine gas with a variety of collision partners was made available by Captain Glen P. Perram, my thesis advisor. This data was generated during experiments conducted in 1984 but had not been analyzed. Analysis of these spectra by means of Stern-Volmer techniques formed the core of this thesis.

In conducting this research, I received a great deal of assistance from others. I am most deeply indebted to Captain Perram for making this data available, his unwavering support through out the conduct of my research, and the countless hours of discussion regarding the techniques and methods applied in this thesis. I also owe special thanks to my faculty advisor, Lieutenant Colonel David Stone, and Professor William Bailey for their support and guidance. Their collective knowledge and experience extended to me in the areas of laser physics, kinetics and spectroscopy greatly assisted my background investigation and final analysis. I also thank Professor Quinn of the Mathematics Department for his assistance provided in conducting my error analysis. Finally, I must thank my wife Nadine for her understanding and support for those many days and nights she spent caring for our children while I was committed to this research.

Table of Contents

List of Figures

List of Tables

ABSTRACT

This study investigated the rotational energy transfer processes of optically excited bromine molecules in the presence of several different collision partners. Resolved laser induced fluorescence spectra of collisionally populated rotational states were analyzed by means of Stern-Volmer techniques. Total rotational removal rate coefficients and state to state rotational removal rate coefficients for the v′=11, J′=35 level of $B^3\Pi(O_u^+)$ state of Br_2 were obtained for collisions with Br_2(X), He, Ar and Xe. Rotational energy transfer rates were also obtained for the (v′=11,J′=26), (v′=11,J′=47) and (v′=14,J′=36) levels of $B^3\Pi(O_u^+)$ states of Br_2 with collisions with Ar. The total rotational removal rate for Br_2 self quenching was found to be $(3.98 \pm 0.2)x10^{-10}$ $[cm^3/molecules-sec]$.

Determination of rotational rates was complicated by the overlap of the P-R doublet in Br2. Deconvolution of rates was performed by application of the exponential gap scaling law with apparently good results. Total removal rates were scaled with respect to reduced mass of the collision system and failed to demonstrate a linear relationship. A strong propensity for rotational energy transfer toward the Boltzmann rotational distribution was observed.

I. INTRODUCTION

1.1 Motivation

The Air Force Weapons Laboratory (WL/ARD) and Strategic Defense Initiative Organization (SDIO) are interested in developing a new class of laser device operating in the visible region under chemical excitation for both directed energy and diagnostic missions. (16:283) Visible lasers offer advantages over other laser devices of equal power operating at longer wavelengths to include reduced beam divergence, higher atmospheric propagation and increased intensity and therefore power on target. Chemically pumped laser devices, free of massive external power supplies, are inherently more compact and offer greater flexibility in deployment and employment. Because visible laser sources offer quasi-continuous wavelength tunability and potential for pulsed or CW operation, they may serve well in a wide range of imaging and diagnostic missions. Visible chemical lasers have also been suggested for use as fusion drivers or as laboratory lasers in future spectroscopic studies. (7:522)

In pursuit of a fully chemical, continuous wave, visible chemical laser, the above agencies manage numerous programs striving toward this goal. One such program is oriented toward the identification and characterization of potential lasant species. This program involves studies including spectroscopy, lasant production kinetics, radiative and collisional dynamics of excited and ground electronic states, and optically pulsed laser demonstrations. These optically pumped laser experiments are proving especially useful in studying the lasant media kinetics under approximated chemical laser conditions. (7:522) The diatomic halogens and interhalogens show particular promise as convenient sources for low power, tunable radiation from the

visible out to $3\mu m$. An optically pumped molecular bromine laser has been demonstrated, but the kinetics of the upper laser level are poorly understood. (17:2526) Specifically, the role of rotational energy transfer in removing energy from the excited electronic state through predissociation is uncertain. (11:408) Rotationally resolved emission from steady-state laser induced fluorescence (LIF) experiments with molecular bromine have been recorded by G.P. Perram as a function of pressure for a variety of collision partners. However, this data has not been analyzed. (18:1) The electronic quenching and total rotational energy transfer rate coefficients for a number of diatomic halogens and interhalogens, including I_2, IF, and BrCl, have been determined through similar experiments involving application of a Stern-Volmer analysis (14:178) to the spectrally resolved laser induced fluorescence data. (19:198) Specific state-to-state rotational rate coefficients for various excited states of I_2 and IF have also been determined for various different collision partners.

1.2 Problem Statement

Analyze the Br_2 $B^3\Pi(O_u^+) - X^1\Sigma_g^+$ steady-state spectrally resolved laser induced fluorescence data from G.P. Perram's experiments to determine selected fundamental physical properties of molecular bromine that are relevant to chemical laser development.

Specifically, the following properties will be determined:

(1) Determine, by application of linear and non-linear Stern-Volmer analysis, the total quenching rates from the optically excited rotational state ($(v_o' = 11, J_o' = 26, 35,$ and 47) and ($v_o' = 14, J_o' = 36$)) for Br_2 with Br_2, He, Ar

and Xe as collision partners. Compare the quenching of total fluorescence and resolved fluorescence from the initially excited state.

(2) Determine rotational removal rates from the optically excited state as a function of vibrational and rotational level for Br_2 with Br_2, He, Ar Xe collision partners.

(3) Determine the total quantum resolved rotational energy transfer rate coefficients as a function of rotational quantum jump ($\Delta J = J_f - J_i$) for the above initially populated states and collision partners.

(4) Apply a common scaling law to the rate coefficients from parts 1-3.

(5) Compare the rotational energy transfer in Br_2 to similar studies in I_2 and IF.

The basic approach to analyzing this CW LIF data is based on similar studies conducted on iodine monofluoride (8:1661). Relative population densities of parent and collisionally populated rotational states will be measured based on recorded emission intensities. Through a Stern-Volmer analysis of these population ratios versus buffer gas pressure, total and state-to-state rotational removal rate coefficients will be extracted. Scaling of these rates will be performed based on reduced mass of collision partner and "energy gap" of collisional rotational energy transfer.

II. Background Theory

2.1 Spectroscopy

Bromine atoms have ground state electronic configurations with outer shells s^2p^5 resulting in $^2P_{3/2}$ and $^2P_{1/2}$ atomic states. Molecular orbitals for molecular bromine are established from a linear combination of atomic states. For halogen atoms the lowest molecular orbital configuration is of the configuration $(\sigma_g)^2(\pi_u)^4(\pi_g)^4(\sigma_u)^0$, abbreviated 2440. (6:180). This configuration comprises the ground electronic state ($^1\Sigma_g^+$). The excited electronic states ($_{1,3}\Pi_u$ and $_{1,3}\Pi_g$) are created from the promotion of an electron to the vacant σ_u orbital.

The spectroscopy of the $B^3\Pi(O_u^+) - X^1\Sigma_g^+$ system for the isotopic species, $^{79}Br_2$ and $^{81}Br_2$, including the 49-0, 50-0, 51-0 and 52-0 bands near the dissociation limit, has been studied by means of chemilluminescence and absorption (3:1992). The absorption spectra recorded by J.A. Coxon (1:428) provide the best recorded spectroscopic constants, potential energy curves and Franck-Condon factors. For the following studies we focus on the $^{79}Br^{81}Br$ isotope of molecular bromine. This isotopic species is most abundant in a given bromine mix ($^{79}Br_2$:$^{79}Br^{81}Br$:$^{81}Br_2$ -> 1:2:1) which allows for the greatest absorption and subsequently greatest fluorescence signal in LIF studies. The presence of three isotopic species does present potential problems in that an already strongly overlapped and dense excitation spectrum may be complicated by emissions from other than the target isotope over the vibrational manifold under investigation. A narrow bandwidth laser is necessary to insure excitation of a single ro-vibrational state. The molecular constants for Br_2 are shown in Table I.

Table I. Molecular constants for the $X^1\Sigma_g^+$ and $B^3\Pi(O_u^+)$ States of $^{79-81}Br_2$. (in cm^{-1}) (1:440)

Constants	Br_2 (X)	Br_2 (B)
T_e	0	15902.47
ω_e	323.3069	166.5688
$\omega_e x_e$	1.0641	1.6159
$\omega_e y_e$	-2.2556x10-3	-9.1957x10-3
β_e	0.081093	0.058853
α_e	3.1285x10-4	4.8007x10-4
γ_e	-1.05x10-6	-6.64x10-6
D_e	2.041x10-8	2.939x10-8
H_e	0	0

A typical potential energy curve for diatomic bromine is shown in Figure 1. Due to the curve crossing of the repulsive ($_1\Pi(1_u)$) state with the bound electronic state $B^3\Pi(O_u^+)$, spontaneous predissociation is observed. Previous studies by Clyne and Heaven have demonstrated a strong rotationally dependent predissociation character of the Br_2 $B^3\Pi(O_u^+)$ state in v'>3 (11:407). This strong predissociative nature makes bromine a poor candidate for LIF studies. This nonradiative loss mechanism has made optical excitation visible laser demonstrations with bromine difficult to perform.

Prior research involving bromine has characterized its performance as a visible lasant species. In figure 2, bromine potential energy curves are again depicted along with various theoretical lasing processes that have been investigated by Wodarczyk and Schlossberg. (23:4478) They demonstrated lasing on fifteen different transitions following pumping on v'=26. G. P. Perram has also demonstrated a molecular bromine laser on J'-J" = 36-29 transition following pumping of v'=14, J'=36.

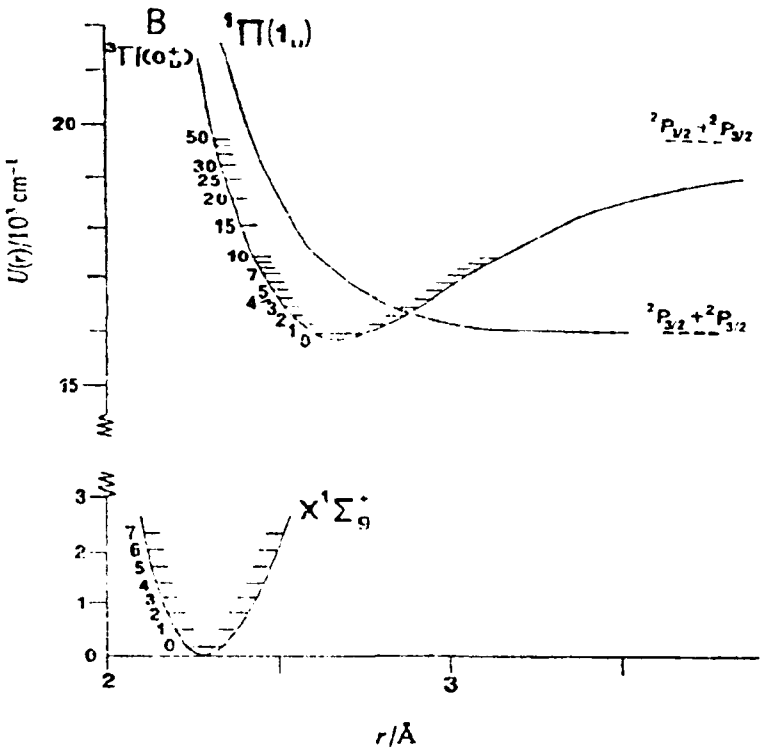

Figure 1. Potential energy curves for Br_2. RKR functions are shown for X state and bound levels of B state. Figure reproduced from Clyne and Heaven paper on Br2 laser excitation studies (3:1993).

(16:286) Simple models developed to characterize the pressure dependence of these bromine lasers predicted lower kinetic quenching rates than previously measured in prior bromine laser excitation studies.

The collisionless decay rate of the Br2(B) state, Γ_o , is determined from the radiative rate, Γ_r , and the nonradiative predissociation rate described by the Kronig function

$$\Gamma_o = \Gamma_r + k_{pd}(v')J'(J'+1) \qquad (1)$$

where $k_{pd}(v')$ denotes a proportionality constant for a given v' and $\Gamma_r = 1/\tau_r$ characterizes the radiative lifetime. (5:1992)

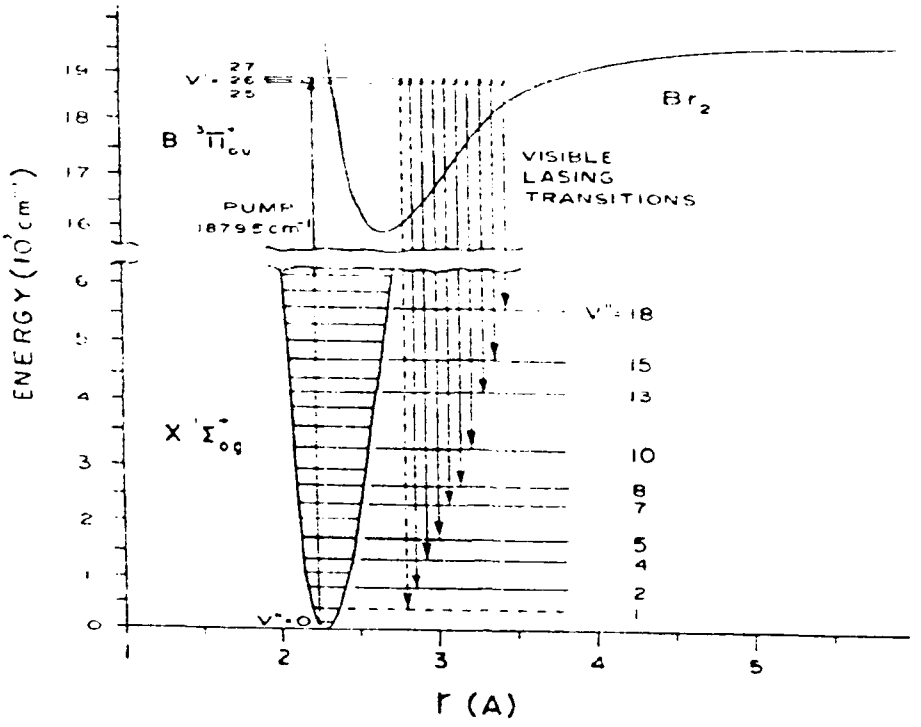

Figure 2. Potential energy diagram indicating excited and ground states of Br_2. This figure highlights the fifteen different lasing transitions investigated by Wodarczyk and Schlossberg following excitation of v'=26. (23:4478)

In equation (1), the predissociation rate coefficient, $k_{pd}(v')$, is strongly dependent upon v' (19:200) and the spontantenous predissociation rate is proportional to J'(J'+1). This relationship is supported by previous lifetime measurement results for Br_2 whose results are depicted in figure 3. The linear dependence of total collisional removal rate with J'(J'+1) supports this dependence. Collisionless lifetimes are therefore strongly dependent upon both vibrational and rota-

tional quantum numbers. In comparison with I_2, predissociation in Br_2 has been observed to be much stronger (by an order of magnitude), however much more uniform across the vibrational manifold. For Br_2 across the range $10< v' <25$, $k_{pd}(v')$ appears to vary slowly.

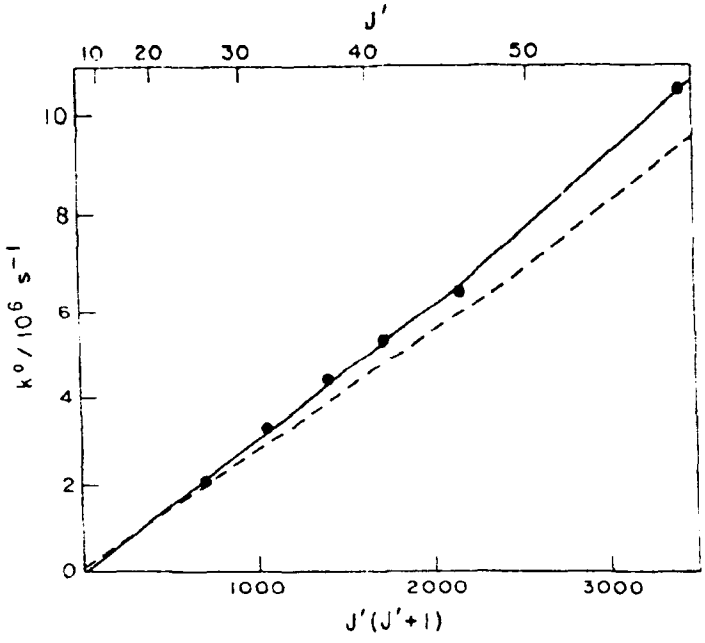

Figure 3. A plot of Br_2 decay rate without collision partners. The solid line shows results obtained by Yamasaki and Leone and the dotted line results by from Clyne and Heaven. (24:971) These studies yielded values $\Gamma_0 = 2.7 \times 10^3 s^{-1}$ for v'=24 (depicted above as k^o) and a mean value of $\tau_0 = 8.1 \mu s$ for $11 < v' < 24$.

The fluorescence yield of an excited state for a homonuclear halogen is described by $\phi_f = k_{fl}/(k_{fl} + k_{pd})$. (21:178) When the predissociation rate is comparable to the radiative decay rate of the species, resolved fluorescence techniques used to examine rotational and vibrational energy transfer become more difficult. Fluorescence quantum yields, inversely dependent

upon k_{pa}, are lower. Detection of collisionally populated "satellite" lines becomes more difficult. Subsequent analysis of line intensity data therefore becomes more difficult. In 1985 G.P. Perram and S.J. Davis succeeded in observing fluorescence from collisional populated rotational states with Br_2 and various collision partners at a variety of pressures. Their data is analyzed in this thesis using techniques explained in following sections.

2.2 Description of Experiment

G.P. Perram conducted an experiment based generally upon a design established in the pioneering energy transfer studies conducted on diatomic iodine by Steinfeld and Klemperer. The general concept is that, upon populating a single excited ro-vibrational quantum state, spontaneous emission can be observed from this initially populated "parent" state as well as adjacent "satellite" lines populated by collisional energy transfer mechanisms. In the absence of collisions, only the initially populated state emissions are observed. When energy transfer collisions occur, emissions from both the parent and collisionally populated satellite levels are observed. Because the resolved fluorescence intensity observed is proportional to the number density of the emitting state, measurements of the relative line intensities of these parent and satellite lines can be used to determine the relative populations of the corresponding emitting states. This data, plus known lifetimes of the excited satellite states, can then be used in a Stern-Volmer analysis to determine the rotational energy transfer rate coefficients.

The laser induced fluorescence apparatus used is shown in figure 4. An Ar^+ ion laser pumped ring dye laser using Rhodamine 590 dye was used to populate a pure ro-vibrational quantum

state of the $^{79}Br^{81}Br$ isotope. The dye laser provided up to 440 mW power with less than 100 MHz (=0.003 cm^{-1}) linewidth. This facilitated selective pumping of (11,35), (11,26), (11,47) and (14,36) ro-vibration parent levels. The fluorescence from the Br_2 sample was spectrally resolved with an 0.3 meter scanning monochromator with about 0.05 nm resolution. Total fluorescence was also monitored using a second photo-multiplier tube. A strip chart recorder was employed to simultaneously record laser induced and total fluorescence data from the chosen sample. Bath gas collision partners, including He, Ar and Xe, were introduced into the fluorescence cell through a variable leak valve connected to a gas handling system. Pressure was effectively monitored using a Baratron capacitance manometer with a 1 torr head and accurately measured pressures to 0.2 mtorr. With this system, Perram observed LIF data with Br_2 and a variety of collision partners at various pressures. (19:57-63, 223-224)

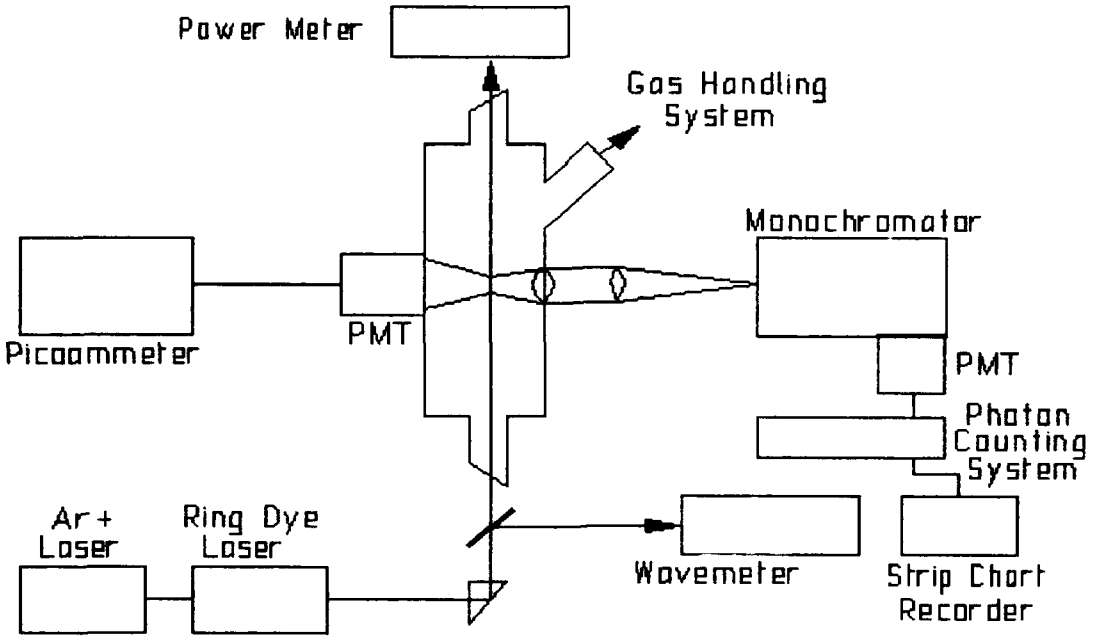

Figure 4. Laser-Induced-Fluorescence (LIF) experimental apparatus. Ar^+ ion laser pumped ring dye laser using Rhodamine 590 dye to populate pure rovibrational state of Br_2. LIF and total fluorescence monitored using PMT's and simultaneously recorded on a strip chart recorder.

$$P(J+1)-R(J-1)=-4B_{v''}\left(J+\frac{1}{2}\right) \qquad (2)$$

Figure 5 shows a typical rotationally-resolved LIF spectrum generated from this experiment. A strong P-R emission doublet arising from the single, initially populated parent level state is easily seen. The weaker satellite transitions observed are from nearby collisionally populated rotational states. Through equation 2, measurements of the separation between the P(J+1) and R(J-1) lines of each doublet, the rotational quantum number J' can be determined. (4:965) An unavoidable problem compensated for in analyzing data created from this system arises

from power variations or frequency drifts in the laser during the fluorescence scanning process. During the 10-20 minutes necessary to conduct one full scan, variations in the input signal could cause considerable variations in the observed fluorescence spectra. During the conduct of the experiment, the total fluorescence was closely monitored during each scan. Whenever the total fluorescence deviated from its straight line "equilibrium" value, indicating a drift in the pump laser frequency, the monitor slightly adjusted the pump laser frequency bringing total fluorescence back to its equilibrium value. Following this procedure for each scan, variations in signal output due to frequency drifts in the pump laser were minimized.

Bromine, like other halogens, emits a strong P-R doublet from the single, initially populated rotational state. As seen in Figure 5, only the ΔJ = Even collisional transitions are clearly observed; every other emission (ΔJ = Odd) appears missing. Quantum mechanical calculations predict transitions involving odd values of ΔJ as symmetry forbidden for homonuclear diatomic molecules. (21:121) The basis for this rule is that the nuclear spin states are not easily altered by collisions. (13:2907) In a homonuclear diatomic molecule, the spin eigenfunctions have a definite parity which alternates with J. A ΔJ = Odd transition would require a simultaneous change of nuclear spin and rotation. Though the $^{79,81}Br_2$ isotope is not a truly homonuclear molecule, McCurdy and Miller have shown that diatomic molecules with nearly identical nuclei demonstrate a strong propensity to follow ΔJ = Even selection rules for small ΔJ. (15:463)

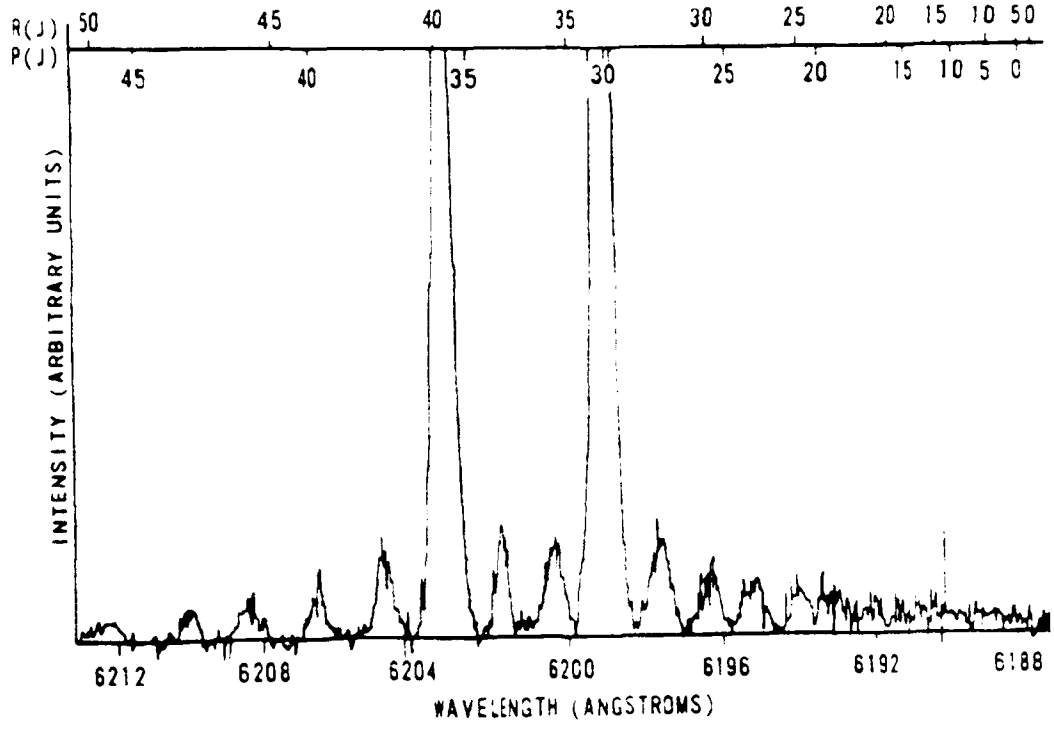

Figure 5. Rotationally-resolved Br_2 CW LIF spectrum. Emission spectrum obtained from pumping $^{79,81}Br_2$ (B:v' = 11, J' = 35) at 26 mtorr Br_2 with 376 mtorr of Ar buffer gas. Note the adherence to the ΔJ = Even collisional selection rule. Each emission line is a blend of an R(J) and P(J-4) line and is therefore proportional to the population of the J' = J+1 and J-5 state.

2.3 Techniques For Analyzing LIF Data

The LIF techniques described below were used extensively by Davis and Holtzclaw in examination of IF spectra (8:1664) and Steinfeld and Klemperer in examining I_2 spectra. (22:3475) This section outlines the specific techniques used to analyze the Br_2 data. Also discussed are various corrective measures taken to account for peculiarities in the experimental apparatus.

2.3.1 Population Determination

A laser is used to optically excite a species populating a particular quantum state J. Collisional energy transfer can then redistribute the initial parent population among other states such as J+1 and J-1. The spectrally-resolved fluorescence from these states yield emission lines that correspond to the parent and collisionally populated satellite levels. The resolved fluorescence intensity is proportional to the number density of the emitting state: (8:1664)

$$I^{v'v''}_{J'J''} \propto N^{v'}_{J'} \nu^4 |R_e|^2 q_{v'v''} \frac{S_{J'J''}}{2J''+1} \qquad (3)$$

where

$I^{v'v''}_{J'J''}$ = emission intensity from state v' to state v"

$q_{v'v''}$ = Franck-Condon factor overlap for states v' & v"

$|R_e|$ = electric dipole moment

$S_{J'J''}$ = rotational linestrength factor

Because of photon counting, the observed intensity is proportional to the cube of the emission line frequency.

A simplified depiction of collisional population of satellite levels is shown in figure 6.

As equation 3 shows, the intensity of a given emission line is directly proportional to the number density of the emitting state. By measuring emission intensities a ratio of population densities from two different emitting states can be expressed by the relation:

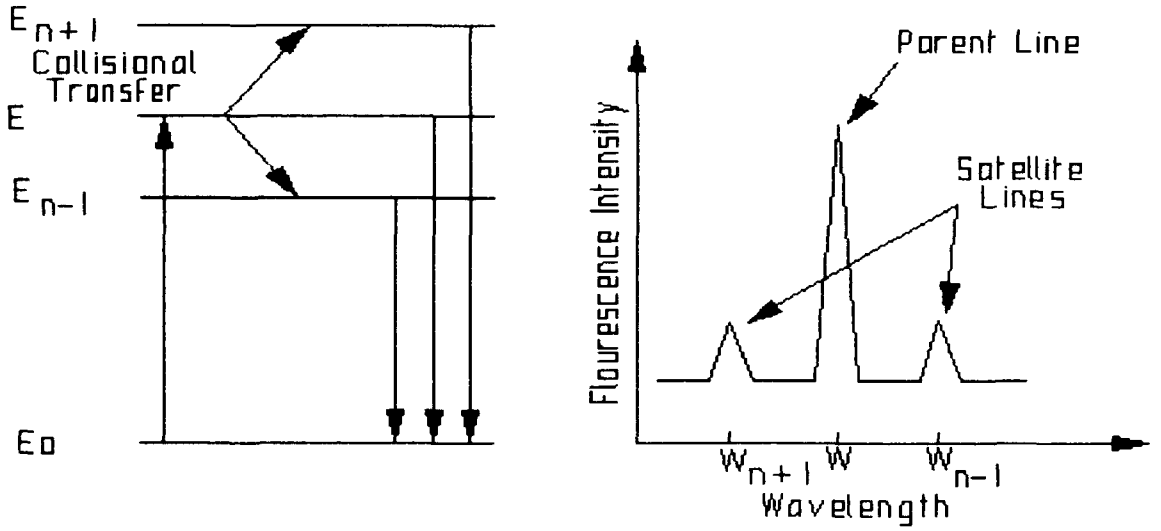

Figure 6. A simplified visual representation of laser induced fluorescence concept depicting typical collisionally populated satellite energy levels and their corresponding spectral emission lines.

$$\frac{N_f}{N_i} = \frac{I_{J_f}(2J_f + 1)(S_{J_i' J_i''})\nu_i^3}{I_{J_i}(2J_i + 1)(S_{J_f' J_f''})\nu_f^3} \tag{4}$$

Similarly, the total fluorescence intensity can be expressed:

$$I_f = \sum_{i'i''} I_{i'i''} = C N_T \tag{5}$$

where $N_T = \sum_i N_i$ and C = proportionality constant.

In determining these population ratios, either measured peak intensities or integrated intensities with respect to wavelength may be used. Accurate use of integrated intensities

involves preparation of digitized LIF spectra, a process involving modification to the experimental apparatus already described. Digitized spectral data was not available from Perram's experiment. However, he did manually estimate the values of areas in his emission spectra. In this study peak height values of emission spectra were used to estimate population densities. In selected cases, the results generated using peak height values were compared to those generated using Perram's estimated area values.

Several problems must be overcome when using measured peak height intensities. As noted earlier, one problem is the overlap of the emission spectra. Figure 5 shows this phenomena common to halogens where the P(J) and R(J+4) lines overlap overlap. This emission line overlap in turn causes calculation of convolved rate coefficients upon application of Stern-Volmer techniques. The technique applied to correct this problem is to derive convolved rate coefficients from the original data, assume a form of the scaling law that may apply to this data, then deconvolve the rate coefficients using this scaling law. The validity of the scaling law chosen can then be checked by "predicting" a convolved emission spectra and comparing this result with the measured data. A close match supports the argument that the scaling law chosen may in fact apply to this case. Application of this technique is discussed in detail later on.

A second problem, also depicted in figure 5, is the loss of spectral resolution near the bandhead where emission lines become more closely spaced. At some point, spectral resolution near the bandhead is lost and identification of specific transitions becomes impossible. This prevents measuring large $+\Delta J = J' - J''$ transitions even if such transitions are observed.

From equation 2, the Br_2 P-R doublet separation is 2.8 Angstroms for J=35. The 0.3 m monochromator used in data collection offered a 0.5 Angstrom resolution. This allows for resolution of the P-R emission doublet for a single populated rotational state for J>14. (19:243)

The measured values used in this study were corrected for the response function of the experimental detection system. Figure 7 shows the spectral response calibration curves for Perram's experimental apparatus. From these curves we define a "detectivity variable", labeled $D(\nu,,)$, which is a function of frequency and corrects the observed emission spectra by $I = I^{obs} D(\nu,,)$. As shown is Figure 7, the relative spectral response was very uniform with a slight slope over the frequency spectrum the Br_2 band was observed. (19:242) A reference wavelength of 6200 angstroms was selected. All peak height intensities measured were corrected for the spectral response of the system based on this reference wavelength and the variation of the relative spectral response. The detectivity function used, as a function of wavelength, is defined as:

$$D(\lambda) = C \frac{\lambda^3}{(0.88 + 0.00021(6200 - \lambda))} \qquad (6)$$

where C = a constant, 0.88 = relative spectral response at 6200 angstroms, and 0.00021 = slope of spectral response curve over the frequency interval under examination, and λ is measured in Angstroms.

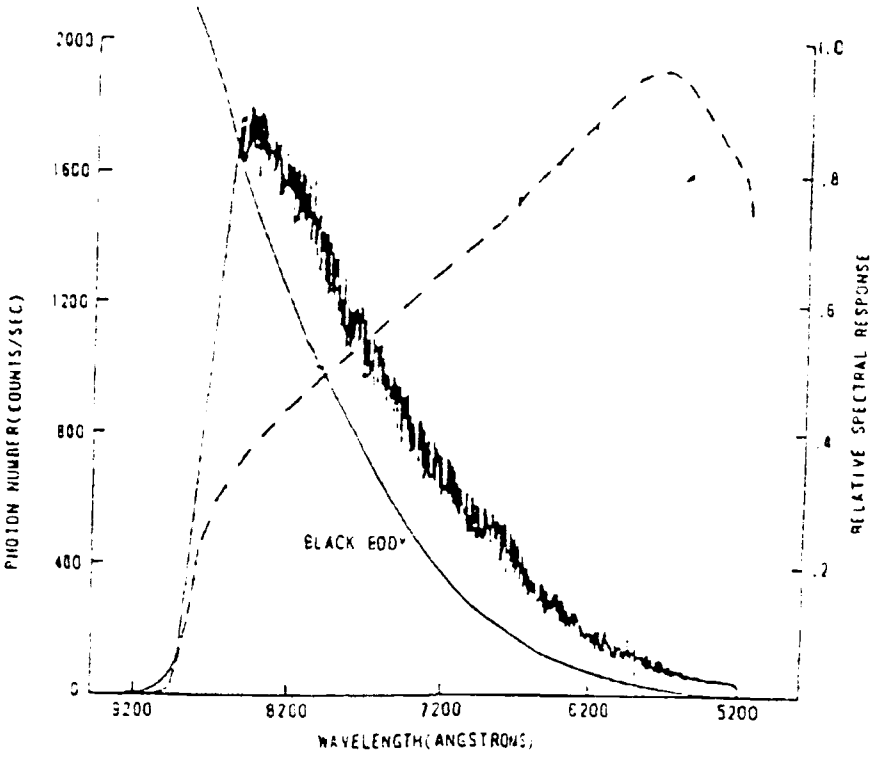

Figure 7. CW spectral response calibration curve, depicted by dotted line, for apparatus used to generate Br_2 spectra. Value of spectral response at 6200 angstroms is 0.88. Spectral response curve is uniform, with slope = 0.00021, over frequency range encompassing Br_2 emissions. The other two curves depict the number of photons counted by λ and a corresponding Planck distribution for blackbody emission.

Measured peak heights were also corrected for variations in total unresolved intensity. As noted earlier, despite careful steps to create the spectral output, variations in input laser intensity were experienced. These variations are experienced in the resolved emission spectra because the observed emission is directly proportional to the pump laser intensity. To correct for these fluctuations in the emission spectra, a base value for total unresolved fluorescence was selected for each spectrum generated. Measured values of peak heights across

this spectra were adjusted in proportion to changes in the total unresolved fluorescence across the same wavelength of the particular feature measured. Figure 8 displays a representative portion of one Br_2 emission spectrum recorded by Perram. The collisionally populated satellite emissions are seen at the bottom and the total unresolved fluorescence is represented by the line across the top of the figure. As this figure shows, the total fluorescence varies over small intervals. A reference point is selected and "scale" for value of total fluorescence established. The measured peak height of rotational line marked P1 in the figure is adjusted by dividing the measured value by the scale value of total fluorescence at that point. The line marked P2 on the other hand does not require an adjustment.

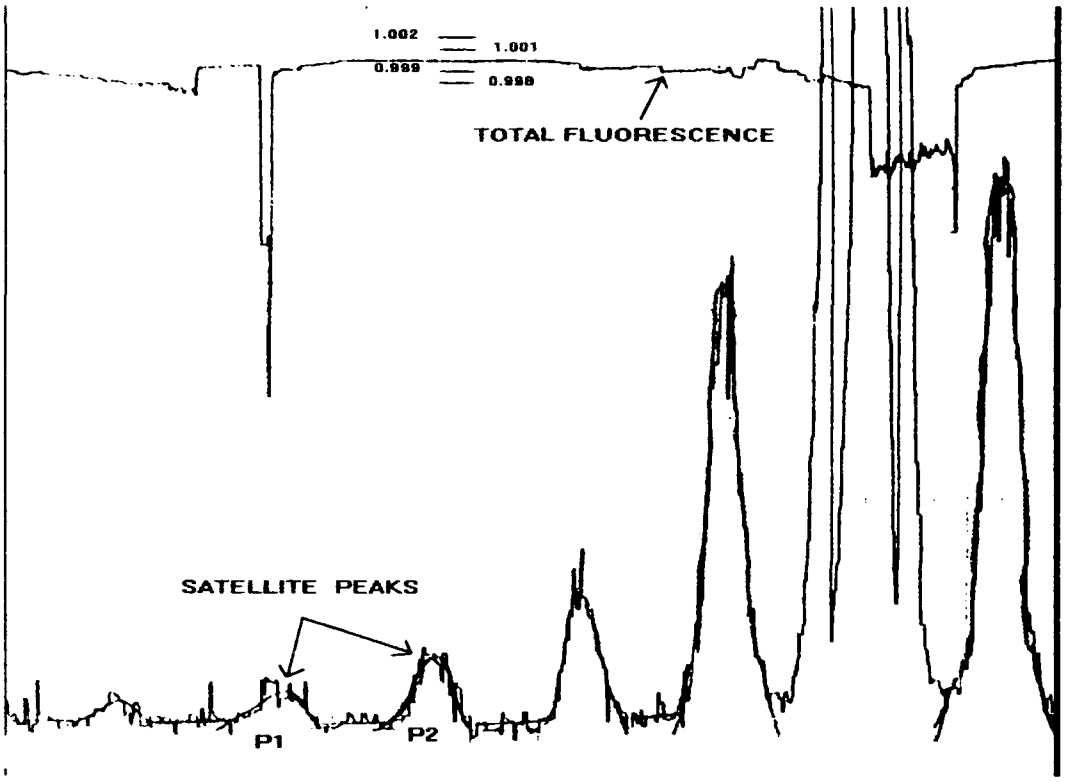

Figure 8. Part of a typical Br_2 emission spectrum. The line near the top reflects the total unresolved fluorescence. Note variations over peak marked P1 and to the right of parent peak (which goes off scale). Peak heights of the satellite lines are measured from a "floating baseline" then are corrected for variations in total fluorescence.

An important consideration was the actual measurement of peak heights. As seen in figures 5 and 8, near the parent lines and near the bandhead, the wings of the emission lines overlap to some degree and sizeable amounts of signal noise is prevalent. To negate the effects of this noise and overlapping signals, a "floating baseline" was used where the zero value on the y-axis scale floated with the signal noise. This is seen in figure 8 around the line labeled P2 where the baseline to the left of this feature is lower than to the right of the feature. The average value of these baselines was used as the

zero point to which the peak height of P2 was measured. Figures 5 and 8 also demonstrate the difficulty of identifying where the peak height is. Numerous "bumps" are clearly evident in the resolved spectra. These fluctuations are, for large values of ΔJ, approach the magnitude of the peak height of particular emission line measured. This creates an uncertainty of up to 25% for some measured peak height values. The implication of such fluctuations is large uncertainties in population ratios which are then propagated through the Stern-Volmer analysis to the rate coefficients.

2.3.2 Kinetic Analysis - Steady State Solution

The following section briefly examines the kinetic processes which are used to interpret the laser induced fluorescence results and ultimately determine the rate constants for rotational energy transfer. Though not all the processes discussed are relevant to the examination of rotational energy transfer, their examination serves to highlight the myriad of competing processes taking place and their interdependence on specific vibrational and/or rotational states. We begin with a brief development of the master rate equation and then examine solution to this equation under steady state conditions.

Our system consists of a dilute gas, $Br_2(B;v'J')$, with many accessible quantum states that may interact with any one or more other chemically inert species M. The Br_2 system under examination was dilute (<50 mTorr of Br_2) in order to maintain the total gas mixture at an equilibrium temperature of 300 °K and attempt to insure only first order processes with respect to $Br_2(B)$ occurred (ie. No $Br_2(B)$-$Br_2(B)$ reactions). Effects of secondary processes are neglected for the time being. The following expressions define the fundamental energy transfer mechanisms pertinent to this study.

Optical excitation of Br_2 to initial excited (parent) state:

$$Br_2(X;v''_o,J''_o)+h\upsilon \xrightarrow{k_p} Br_2(B;v'_o,J'_o) \tag{7}$$

Stimulated emission from excited state

$$Br_2(B;v',J')+h\upsilon \xrightarrow{B_{10}} Br_2(X;v'',J'')+2h\upsilon \tag{8}$$

Spontaneous emission from excited state:

$$Br_2(B;v',J') \xrightarrow{A} Br_2(X;v'',J'')+h\upsilon \tag{9}$$

Predissociation of excited state:

$$Br_2(B;v',J') \xrightarrow{k_{pd}} 2Br(2P_{3/2}) \tag{10}$$

Electronic quenching of excited state:

$$Br_2(B;v',J')+[M] \xrightarrow{k_{eq}} Br^*_2+[M] \tag{11}$$

Vibration-Translation (V-T) energy transfer:

$$Br_2(B;v')+[M] \xrightarrow{k^M_{VT}(v',\Delta v)} Br_2(B;v'+\Delta v)+[M] \tag{12}$$

Rotation-Translation (R-T) energy transfer:

$$Br_2(B;v',J')+[M] \xrightarrow{k^M_{RT}(v',J'+\Delta J)} Br_2(B;v',J'+\Delta J)+[M] \tag{13}$$

Ro-vibrational energy transfer:

$$Br_2(B;v',J')+[M] \xrightarrow{k^M_{VT}} Br_2(B;v'+\Delta v,J'+\Delta J)+[M] \tag{14}$$

Equation (7) describes the optical excitation process where the target species, Br_2, is excited to a specific quantum state (v′,J′) by absorbing monochromatic radiation provided by the pump laser. This initially populated excited state is the "parent" state. The pump rate constant, defined as

$$k_p = \left(B_{01} \frac{I_0}{c} \right) \int_0^\infty a(\upsilon) g_p(\upsilon) d\upsilon \qquad (15)$$

where

B_{01} = Einstein coefficient for stimulated emission

I_0 = Incident pump laser intensity

c = speed of light

$a(\upsilon)$ = Absorption transition linewidth function

$g_p(\upsilon)$ = Pump laser linewidth function

The dye laser utilized in generating the Br_2 data in this study had a linewidth of 100 MHz (0.0033 cm^{-1}). This is narrower than the single J level Br_2 absorption bandwith of 0.02 cm^{-1}. This ensured doppler limited excitation of a single rotational parent state.

Stimulated emission, depicted by equation (8), is essentially the inverse of optical excitation. These two processes can be combined into a single relation, S, which represents the net pumping rate: (19:28)

$$S\delta_{\upsilon,\upsilon_0}\delta_{J,J_0} = \frac{B_{01} I_0}{c} \left(N(X;\upsilon''_0, J''_0) - \frac{g_0}{g_1} N(B;\upsilon'_0, J'_0) \right) \delta_{\upsilon,\upsilon_0}\delta_{J,J_0} \qquad (16)$$

where

g_1, g_0 = degeneracies of excited (1) and ground (0) states

$N(X;\upsilon''_0, J''_0)$ = Concentration of Br_2 ground state

$N(B;\upsilon'_0, J'_0)$ = Concentration of Br_2 excited state

δ_{ij} = Kronecker delta function

Previous studies with halogens have found the B-X transition moments to be small. (19:28) The pump term is much larger than the stimulated emission term. The net pump rate, S, is therefore dominated by the pump term and directly proportional to the Br_2 concentration. Close examination of S high-

lights a problem that must be avoided when conducting LIF experiments, saturation. Saturation can lead to artificially high excited level populations making studies of energy transfer mechanisms useless using LIF techniques. If the species under investigation suffers from saturation during CW LIF studies, the population density of the "parent" state, N_1, is effected. When fully saturated, an excited molecule that naturally de-excites to the ground state is immediately pumped again to the excited state. The population ratio N_2/N_1 is then dependent of the rate of excitation rather than the decay rate of the excited state. In this study, the incident pump intensity was an order of magnitude less then that required to achieve saturation.

Spontaneous emission, described by equation (9), is a collisionless process where the excited state undergoes radiative decay. The rate for this process is dependent upon the excited state population and einstein coefficient, A, governing the transition. (19:29)

$$A(v',J' \rightarrow v'',J'') = \left(\frac{64\pi^4}{3hc^3}\right) |R_e|^2 q_{v'v''} \frac{S_{J'J''}}{2J''+1} \tag{17}$$

The radiative lifetime, τ_r , from state v' to v" is defined by: (6:210)

$$\frac{1}{\tau_r(v')} = A(v') = \sum_{v''J''} A(v',J' \rightarrow v''J'') \tag{18}$$

which highlights the radiative lifetimes dependence on specific quantum states (v',J';v"J"). Radiative lifetime measurements have been made on Br_2 (B-X) transitions by Coxon and more recently by Clyne and Heaven. (3:2009)

Due to its negative effect on emission signal intensity, predissociation, described by equation (10) and discussed earlier in section 2.1, is a collisionless process of concern. Clyne and Heaven's laser excitation studies with Br_2 have shown a predissociative behavior for v'>3 with a dependence upon both v' and J'. Unlike results from similar studies with I_2, the predissociative rate constant, $k^{pd}(v')$, varies slowly over the vibrational range 10 < v' < 25. (3:1992) Using equation 1 we can express the total collisional decay rate of Br_2, Γ_0 , by the relations:

$$\Gamma_0(J') = \frac{1}{\tau_0} = \Gamma_r + k_{pd}(v')J'(J'+1) = \frac{1}{\tau_r} + \Gamma_{pd} \tag{19}$$

In this work, the Clyne and Heaven measured values of $\tau_r = 8.1^{+5.4}_{-2.4}\mu s$ for v' = 11 and 14 are used in this study (5:2009)

Electronic quenching, described in equation (11), is a collisional energy transfer process referring to the removal of thermalized $Br_2(B)$ to a lower electronic state. The total electronic quenching rate also incorporates resonant electronic exchange and is defined as (19:31)

$$k_q = k_{eq} + k_{ee} \tag{20}$$

Vibration-translation energy transfer, equation (12) describes the collisional transfer of energy to the parent species displacing from vibrational state v' to state v' + Δv. Similarly, rotational energy transfer, equation (13) describes collisional energy transfer to the parent species moving it from the parent J' state to satellite $J' + \Delta J$ states within the parent vibrational band. The rate constants for total rotational removal from vibrational state v' and rotational state J' are described by the relations (19:31)

$$k_t^M(v') = \sum_{\Delta v} \sum_{\Delta J} k_t^M(v' \rightarrow v' + \Delta v, J' \rightarrow J' + \Delta J) \tag{21}$$

$$k_J^M(J') = \sum_{\Delta J} k_t^M(J' \rightarrow J' + \Delta J) \tag{22}$$

The total removal rate incorporating the collisional and quenching mechanisms described is expressed by

$$k_R^M(v') = k_v^M(v') + k_q^M(v') \tag{23}$$

$$k_R^M(v', J') = k_R^M(v') + k_J^M(J') \tag{24}$$

By incorporating all the energy transfer processes discussed, a master rate equation modeling the time rate of change of the $Br_2(B;v'J')$ number density for a given quantum state:

$$\begin{aligned}\frac{dN(B;v'J')}{dt} = {} & S\delta_{v'v'_0} - \Gamma_0(v'J')N(B;v'J') \\ & - \sum_M k_q^M(v'J')[M]N(B;v'J') \\ & - \sum_M \sum_{\Delta v} \sum_{\Delta J} k_v^M(v' \rightarrow v' + \Delta v, J' \rightarrow J' + \Delta J)[M]N(B;v'J') \\ & + \sum_M \sum_{\Delta v} \sum_{\Delta J} k_v^M(v' + \Delta v \rightarrow v', J' + \Delta J \rightarrow J')[M]N(B;v' + \Delta v, J + \Delta J)\end{aligned} \tag{25}$$

For a continuous-wave laser source the population of any given excited state reaches a steady-state whose population density is constant and therefore independent with respect to time.

$$\frac{dN(B;v'J')}{dt} = 0 \tag{26}$$

Which presents a condition we apply to the master rate equation in the next section.

2.3.3 Linear Stern-Volmer Analysis

The use of Stern-Volmer plots to determine rotational removal rates and various rate coefficients was pioneered by Steinfeld and Klemperer in their I_2 studies. A relatively simple, first-order technique, it has since been successfully applied by numerous others in examining a variety of halogens and interhalogens with minor modifications. (8:1663-1664)

From the steady state analysis results in section 2.3.2 and under single-collision conditions, the steady state population of any rotationally populated state is defined by

$$\frac{dN(J)}{dt} = N(J_0)[M]k_J(J_0,J) - \frac{N(J)}{\tau_0(J)} = 0 \tag{27}$$

where N(J) is the final rotationally populated state density, N(Jo) is the initially populated parent state density, [M] is the bath gas density, $\tau_0(J)$ is the radiative lifetime of the final state and $k_J(J_0,J)$ is the state-to-state rotational transfer rate coefficient. This expression can be re-expressed in the form

$$\frac{N(J)}{N(J_0)} = [M]k_J(J_0,J)\tau_0(J) \tag{28}$$

Plotting $N(J)/N(J_0)$ versus $[M]\tau_0(J)$, where [M] is represented by the bath gas pressure, yields a linear function with a y-intercept at zero. The slope of this function is $k_J(J_0,J)$. Rotational rate constants for each observable transition (J_o->J) are then calculated by measuring and plotting N(J)/N(J_o) vs pressure.

2.3.4 Corrections for Non-Linear Processes

The analysis presented in the previous section accounts for rotational transfer mechanisms only. A first order correction to equation (28) involves accounting for other non-rotational energy transfer processes to include electronic quenching, predissociation and vibrational transfer. (8:1663) This approximation allows for R-T removal from J_i to all other rotational levels within v_i. Upon considering these additional energy transfer mechanisms, equation (29) can be re-expressed as

$$\frac{N(J_f)}{N(J_0)} = k_J(J_0, J_f)[M]\tau_0(J)/(1+\alpha) \tag{29}$$

where

$\alpha = k_R[M]\tau_0(J_f)$

k_R = The total removal rate from state J_f to all other J within v'

Previous experiments have shown that at low pressures, $\alpha \ll 1$, and the relative populations follow a linear dependence with respect to pressure. However, at higher pressures, curvature in Stern-Volmer plots is observed. (18:6) This behavior is demonstrated in figure 9 regarding Davis and Holtzclaw's studies with IF.

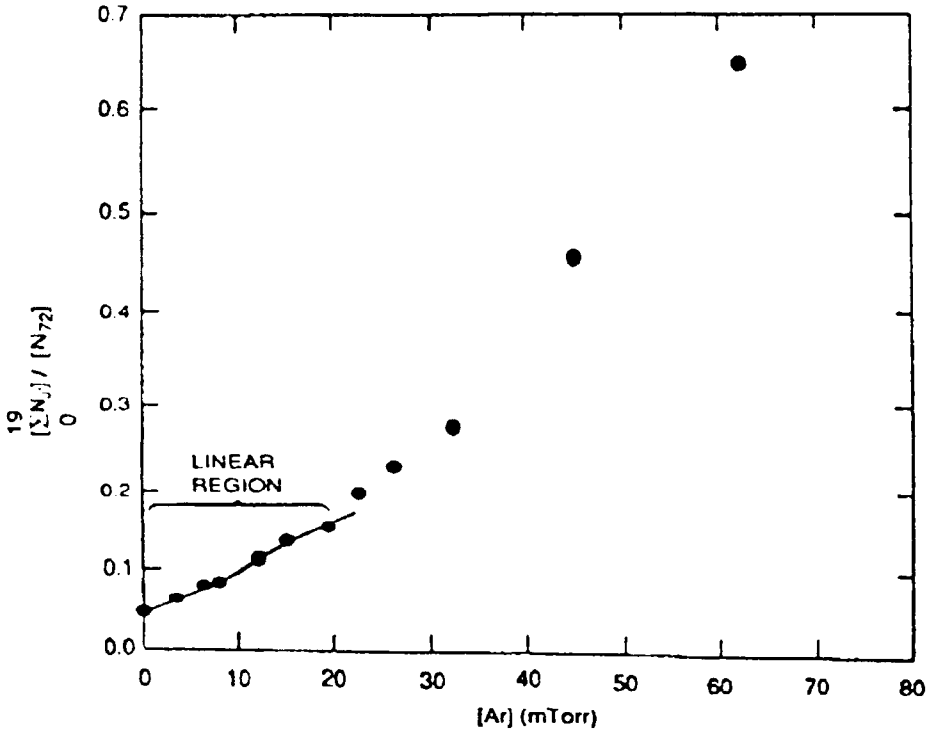

Figure 9. Stern-Volmer plot from IF laser induced fluorescence studies by Davis and Holtzclaw. The plot of $\sum N_J'/N_{J=72}$ versus [Ar] (mTorr) shows linear behavior for low pressures (<20 mTorr) and nonlinear behavior at higher pressures indicative of secondary collisions. (8:1664)

A possible correction for the nonlinear dependence introduced by α can be made if a value for k_R is known. For an answer to this problem we address total quenching rates.

Total quenching rates can also be obtained from linear Stern-Volmer plots. The ratio of the observed intensity at a given buffer gas pressure to the intensity at zero buffer gas pressure is given by: (18:4)

$$N(J_0)_{M=0}/N(J_0) = 1.0 + k_Q^M[M]/(\Gamma_0 + k_Q^{Br2}[Br2]) \quad (30)$$

where Γ_0 is the collisional decay rate, k_Q^{Br2} the self quenching rate coefficient and k_Q^M is a buffer quenching rate coefficient. Plotting $N(J_0)_{M=0}/N(J_0)$ versus [M] will yield a linear relation whose slope is k_Q^M. This analysis offers the advantage in that it can be applied to both unresolved fluorescence and resolved fluorescence from the initially excited state. Application of this technique requires the assumptions that Γ_0 is state independent and that the radiative lifetime for these states to be independent of vibrational state (v'). These assumptions have been successfully applied to studies with IF(B) and BrCl(B) and verified by experimental results. (19:36) The resulting quenching rates (k_Q^M) are expected to be nearly gas kinetic and, in the case of resolved fluorescence, which include the total rotational energy removal rate, k_R. (18:4) (We can approximate k_R with the value for k_Q^{Br2} obtained from analysis of $Br_2(B)$-$Br_2(X)$ self quenching data.)

With a value for k_R we can return to equation (30) and plot population ratios versus $[M]/(1+\alpha)$. Provided the effects of secondary collisions are not severe, this approximation serves to "straighten out" the nonlinear Stern-Volmer plots in low pressure ranges. This approximation was introduced and successfully employed by Steinfeld and Klemperer in their I_2 studies. (22:3483). Results of this technique applied to Perram's bromine experiments are shown in Figure 10. Note in this figure the nonlinear relationship between population ratio and [M] and how the "corrected" data appears to re-establish a linear relation.

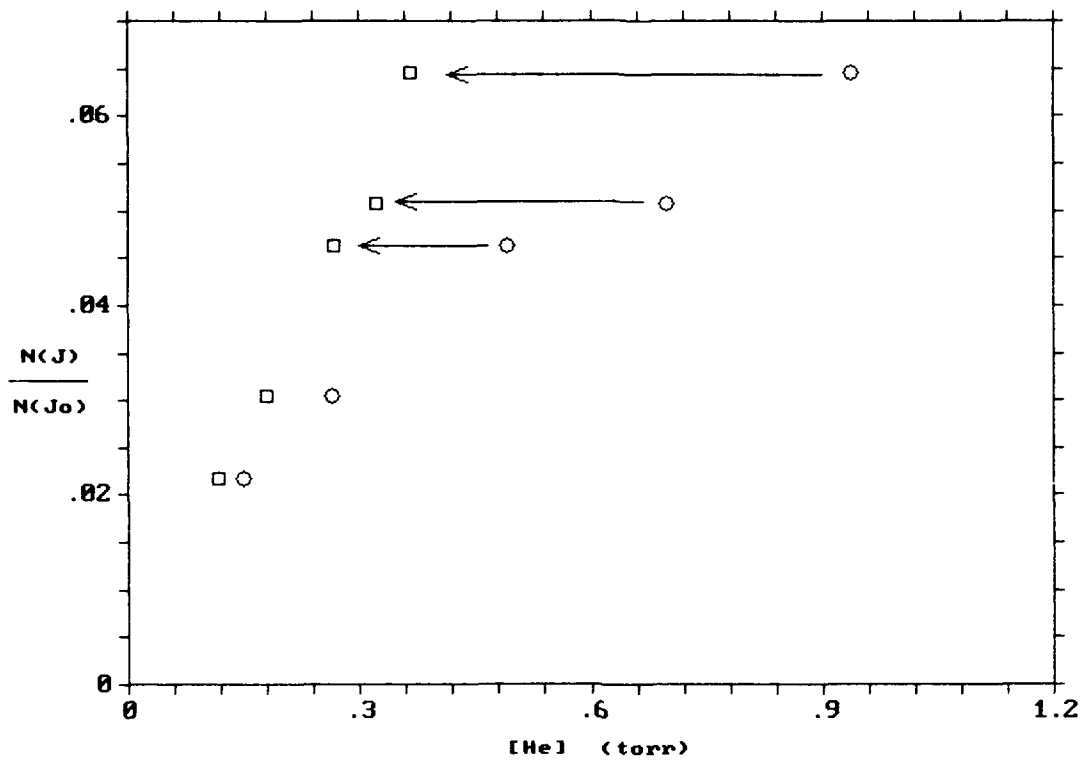

Figure 10. Plot shows Br2-He rotational transfer for Jo=35 -> J-41. Note nonlinearity in uncorrected data (circles) and how incorporation of α factor appears to "straighten out" data (squares). Closer inspection shows corrected data points at higher pressures are actually "over corrected".

A shortfall for this α factor, 1st order approximation is that it does not allow for the repopulation of J_F via a secondary collisions from intermediate rotational levels. When secondary collisions occur, intermediate satellite levels are populated from secondary collisions with neighboring intermediate levels as well as from the parent level. Larger ΔJ's from the initially populated parent state are affected more than small ΔJ's as there are more combinations of intermediate states to populate the final state. The first order

correction explained above tends to "over correct" for secondary conditions when repopulation is not considered. A closer look at figure 10 shows that the lower pressure corrected data points appear linear but at higher pressures, the corrected data points depart from linearity. These population ratios are "over corrected". This behavior is even worse for larger ΔJ's where fewer data points are collected and greater uncertainties exist in fitting functions to this data.

Demtroder and Bergman accounted for these secondary collisions in their Stern-Volmer analysis of Na_2 data. (9:596) They use a similar approach as described above where α is defined as

$$\alpha = \left\{ k_R^T[M] - \sum_{i \neq f} k_R(i \rightarrow f) \left(\frac{N_i}{N_f}[M] \right) + k_v[M] + k_Q[M] \right\} \tau_r \qquad (31)$$

The additional summation term accounts for repopulation of J_f via secondary collisions and serves to counteract the removal from J_f via the RT removal term, $k_R^T[M]$. In previous studies, multiple collisions are treated using the above equation following an iterative approach. For each J_f, a plot of $N(J_f)/N(J_i)$ vs [M] is created from which an initial value of $k_R(i->f)$ is obtained. Using this value, α is calculated and a modified $N(J_f)/N(J_i)$ plot created. A new value for $k_R(i->f)$ is obtained and the process is repeated until values for $k_R(i->f)$ converge. This procedure was applied in Davis and Holtzclaw's studies with IF. (8:1664) This approach has the potential to be very laborious and can introduce large uncertainties.

An alternative, more simplified approach is presented below which accounts for these same secondary processes but with

somewhat less rigor. We return to the steady state solution of the master rate equation incorporating the additional J_t repopulation term. Under steady state conditions

$$dN\frac{(J)}{dt} = k(J_0 \rightarrow J)N(J_0)[M] - N(J)\{\Gamma_0(J) + k_R(J)[M]\}$$
$$+ \sum_t k(J_t \rightarrow J)N(J_t)[M] = 0 \qquad (31)$$

As shown earlier, we create the population ratio

$$\frac{N(J)}{N(J_0)} = \frac{k(J_0 \rightarrow J)[M] + \sum_t k(J_t \rightarrow J)[M]\frac{N(J_t)}{N(J_0)}}{\Gamma_0(J) + k_R(J)[M]} \qquad (33)$$

By dividing the numerator and denominator on the right side by Γ_0, factoring out N(J)/N(Jo) from the right side of the equation above and a little rearranging, we get

$$\frac{N(J)}{N(J_0)} = \frac{\frac{k(J_0 \rightarrow J)}{\Gamma_0(J)}[M]}{1 + \frac{k_R(J)}{\Gamma_0(J)}[M] - \sum_{t \neq 0} \frac{k(J_t \rightarrow J)}{\Gamma_0(J)}\frac{N(J_t)}{N(J)}[M]} \qquad (34)$$

This relation is similar to the first order correction relation to the linear Stern-Volmer analysis described earlier. We also apply this relation in a similar manner. By approximating the value of k_R with the total removal rate determined from Br_2-Br_2 self-quenching data, and by using known values for [M] and $\Gamma_0(J)$, the above equation can be simplified to the nonlinear form

$$\frac{N(J)}{N(J_0)} = \frac{ax}{b+cx} \tag{35}$$

where b = constant close to 1; x = bath gas pressure; cx accounts for the various secondary collision effects described earlier; and the constant "a" holds the rotational rate constant we are seeking. Upon plotting the population ratio versus bath gas pressure we apply a least squares fit to this data using the above nonlinear fitting function with two unknowns, a and c. Upon finding a value for a, we extract the desired rotational rate constant through the expression

$$k_R(J_0 \rightarrow J) = a\Gamma_0(J)d \tag{36}$$

where d = conversion constant required to convert units of pressure to population density.

This fitting function has the advantage of "forcing" a value of zero for the population ratio at zero buffer gas pressure. This a logical effect since collisional energy transfer doesn't occur if there aren't any collisions.

This approach is valid if the summation term

$$\sum_{i \neq 0} \frac{N(J_i)}{N(J)} \tag{37}$$

is not a function of [M]. If this sum is a function of [M] then the population ratio is of the form

$$\frac{N(J)}{N(J_0)} = \frac{ax}{b + cx + dx^2} \tag{38}$$

For low pressures where secondary collisions are present but not to a significant degree, the summation term is small compared to the remaining values in the denominator. Both nonlinear forms described yield the same values for a and the same rotational rate constants. Such was the case in the analysis of the Br_2 data in this thesis.

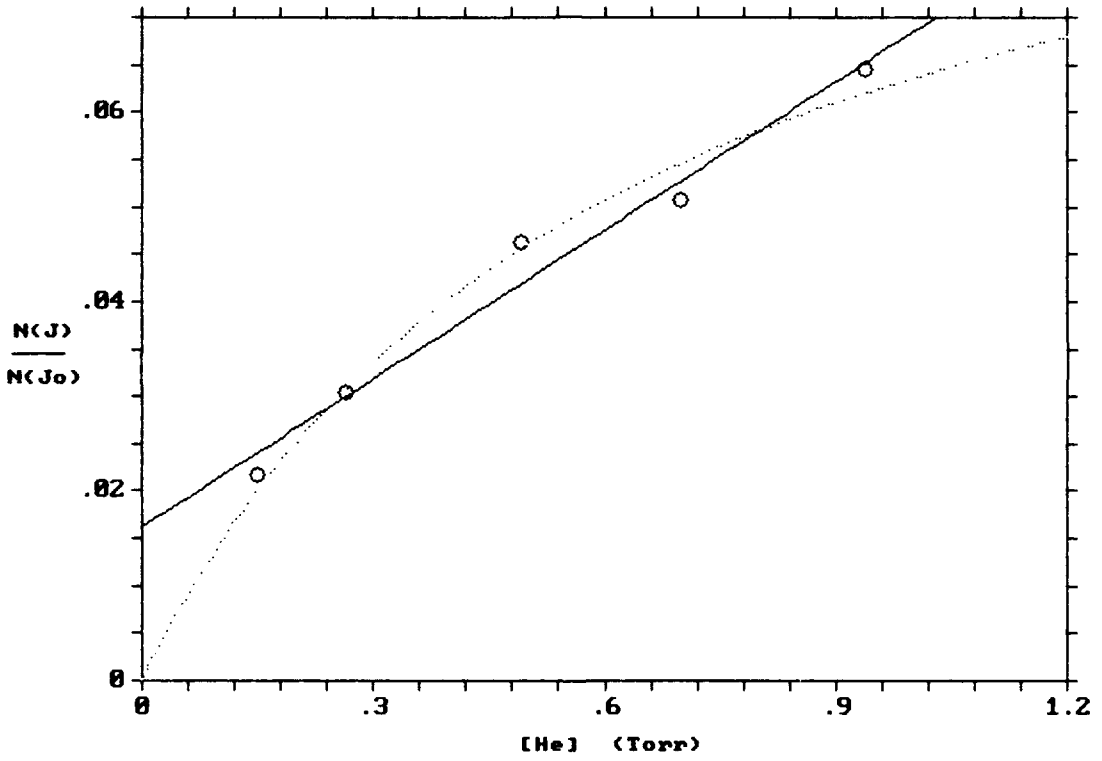

Figure 11. Stern-Volmer plots comparing linear vs nonlinear approach for Br2-He data. Plot depicts measured population ratios for (Jo=35 -> J=39) transition.

Figures 11 and 12 demonstrate this nonlinear approach as applied to Perram's bromine data. As these figures show, the

nonlinear fitting functions "fit" the measured population ratios significantly better than the linear Stern-Volmer analysis approach.

State-to-state rotational removal rates for foreign gas partners were obtained by application of this nonlinear Stern-Volmer technique. Results are tabulated in the Results section.

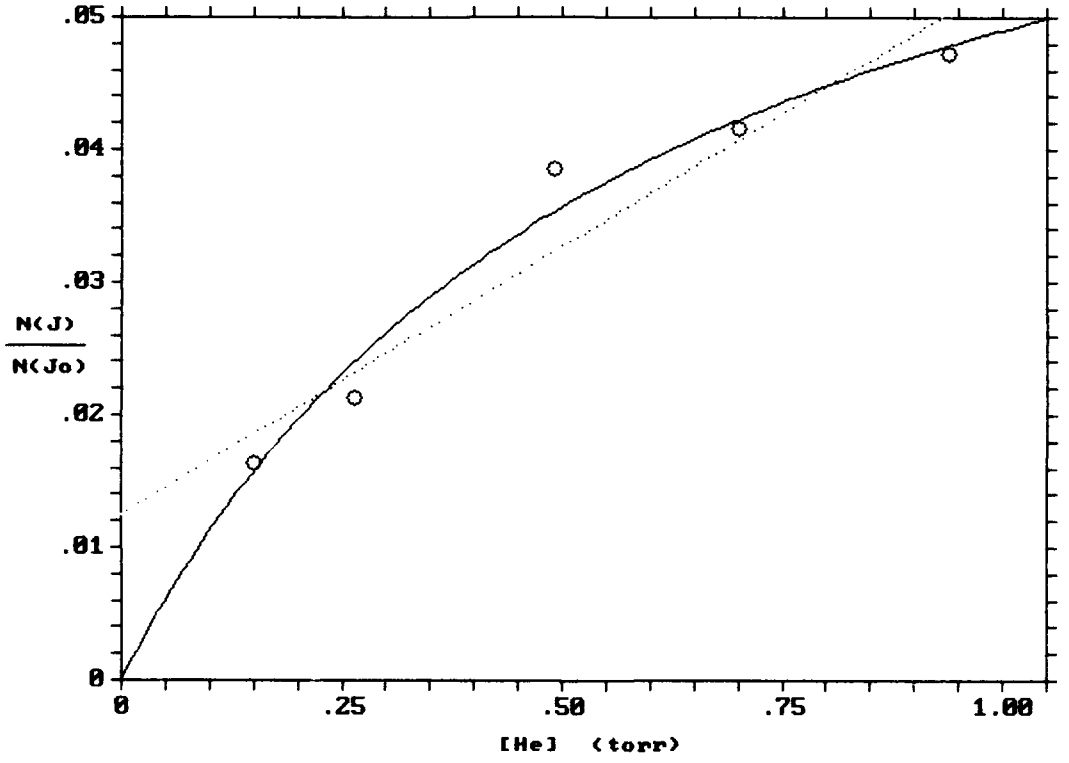

Figure 12. Stern-Volmer plot for Br2-He (Jo=35 -> J=41) transitions. Comparison of linear vs nonlinear approach.

III. Data Reduction

Perram successfully recorded spectrally resolved fluorescence from optically excited Br_2 using a variety of collision partners. Emission spectra were obtained from optically pumping $Br_2(B:v'=11,J'=35)$ using collision partners $Br_2(X)$, He, Ar and Xe. Additional spectra were also obtained by optically pumping $Br_2(B:v'=11,J'=26)$, $Br_2(B:v'=11,J'=47)$ and $Br_2(B:v'=14,J'=36)$, each using Ar as the collision partner. Recorded emission lines were identified from recorded spectra by identifying the wavelength corresponding to each line. Predicted values for these emission lines, calculated using spectroscopic constants from table I and corrected for air, are listed in appendix A.

3.1 Self Transfer Case

For the self-transfer case, we examine rotational energy transfer for $Br_2(B):Br_2(X)$ collisions. The $Br_2(B:v'=11,J'=35)$ state was optically excited and six emission spectra were generated for bromine pressures ranging from 124 mTorr to 1450 mTorr. Total removal rates were calculated from both the total resolved fluorescence data and total unresolved fluorescence data. State-to-state rotational rate coefficients were then calculated by means of linear Stern-Volmer techniques described earlier.

3.1.1 Total Removal Rates

From the $Br_2(B):Br_2(X)$ emission spectra values of total unresolved fluorescence intensity were measured for each pressure. The value of total fluorescence is described by the relation

$$\frac{1}{I_{TF}} = \frac{\Gamma_0(J)}{S_0}\left(\frac{k_q}{\Gamma_0} + \frac{1}{[Br2]}\right) \tag{39}$$

where S_o is a source term due to optical pumping of the excited state, k_q is the total removal rate, and $[Br_2]$ is bromine concentration. This expression is of the simple form $y = mx + b$ where x represents $1/[Br_2]$. By plotting 1/Intensity versus 1/Pressure we can calculate numerical values for the slope and intercept, m and b. From equation (39), the ratio of the intercept to the slope is

$$\frac{a}{m} = \frac{k_q}{\Gamma_0} \tag{40}$$

from which we solve for the total removal rate

$$k_q^{Br2} = \Gamma_0 \left(\frac{a}{m} \right) \tag{41}$$

Applying this technique to the measured total unresolved fluorescence, a total rotational removal rate of $k_R^{Br2} = (3.3 \pm 0.4) x 10^{-10}$ [cm³/molec-sec] was obtained.

This same technique is applied using total resolved fluorescence data. In this case, the peak height value of the parent (J_o) emission line is used instead of the total unresolved intensity. By this method a total removal rate was determined to be $k_q^{Br2} = (3.98 \pm 0.20) x 10^{-10} [cm^3/Molecule-Sec]$. The Stern-Volmer plot for calculation of total rotational removal rate from total resolved fluorescence is shown in Figure 13. This value above is somewhat lower than the lower bound rate of $4.4 x 10^{-10}$ calculated by Clyne, Heaven and Davis in their bromine studies. (4:973)

The total removal rate calculated from total unresolved fluorescence is less than that calculated from total resolved fluorescence. This result is expected because the observed total unresolved fluorescence does not account for nonradiative transfer from one rotational state to another. This loss mechanism is accounted for in measurements of the resolved fluorescence of the parent line.

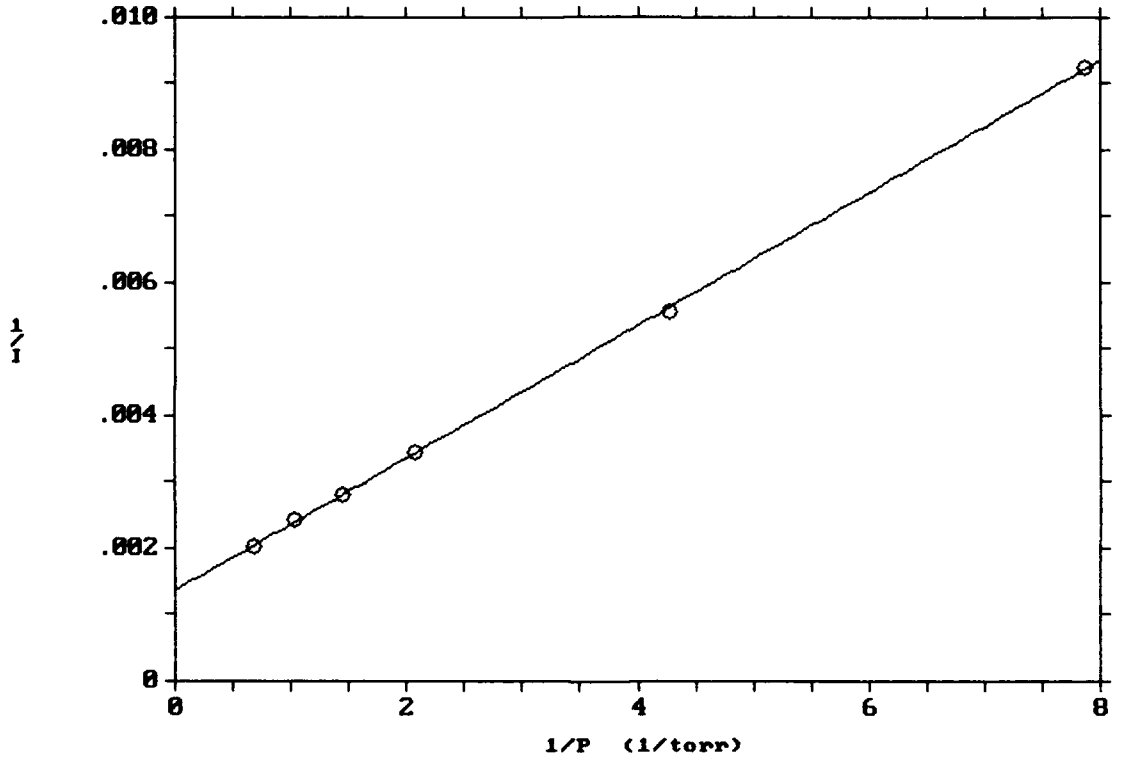

Figure 13. Stern-Volmer Plot of Br2(B)-Br2(X) for calculation of total resolved fluorescence.

3.1.2 State-to-State Rotational Removal Rates

In calculating the state-to-state rotational removal rates in the self quenching case, the same linear Stern-Volmer techniques discussed earlier were applied. However, since a for-

eign collision partner does not exist, the rate equations are slightly different. For the self transfer case, the applicable rate equation is

$$\frac{dN(J)}{dt} = N(J_0)[Br_2]k_J(J_0, J) - \frac{N(J)}{\tau_R} \tag{42}$$

where

$$\Gamma(J) = \frac{1}{\tau(J)} = \left\{ k_v \cdot J''(J''+1) + \frac{1}{\tau_R} + k_R^{Br2}[Br2] \right\} \tag{43}$$

Under steady state conditions, dN/dt = 0. Applying this condition and defining the relation

$$\alpha = k_v \cdot J''(J''+1) + \frac{1}{\tau_R} \tag{44}$$

we generate the population ratio

$$\frac{N(J)}{N(J_0)} = \frac{k_R(J_0, J)[Br2]}{\alpha + k_R^{Br2}[Br2]} \tag{45}$$

which we can rearrange and express as

$$\frac{N(J_0)}{N(J)} = \frac{1}{[Br2]}\left\{ \frac{\alpha}{k_R(J_0, J)} \right\} + \frac{k_R^{Br2}}{k_R(J_0, J)} \tag{46}$$

Equation (46) is again of the desired form y = mx + b where x = 1/Pressure. Plotting the population ratio N(Jo)/N(J)

versus 1/[Br2] and fitting a straight line to this data gives us values for both the slope and intercept. Using known values for α we can calculate the individual rotational rate coefficients from the value of the slope. Using the total rotational removal rate for bromine calculated earlier, we can also calculate the individual rotational rates from the values of the intercepts. In this study, the rates calculated from the slope and intercept values are generally the same for small ΔJ, but varied by about 10% for larger ΔJ. The numerical error bounds for the rotational rates calculated from intercept values of the Stern-Volmer plots were larger than those calculated from slopes. Rotational rate coefficients tabulated in Results section represent those calculated from slopes of Stern-Volmer plots.

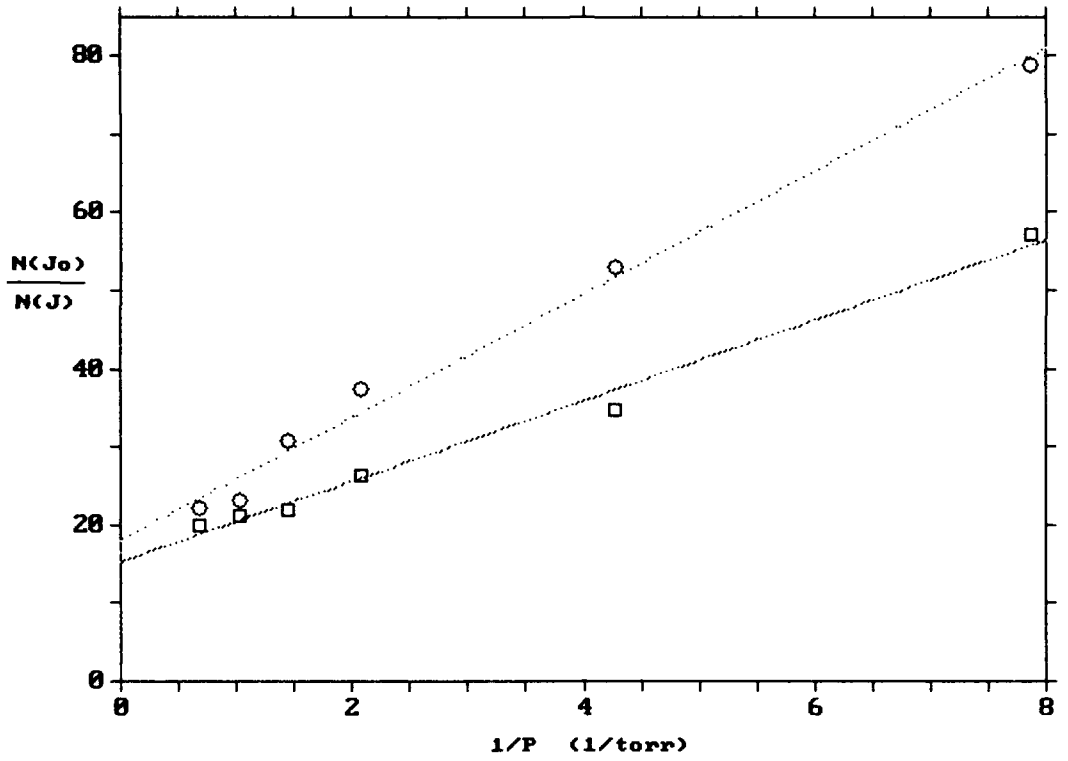

Figure 14. Stern-Volmer plot of bromine self quenching case for Jo-35 -> J=27. Plot compares measured peak heights vs area data for computation of population ratios. Upper curve is fit to peak height data; lower curve fit to area data.

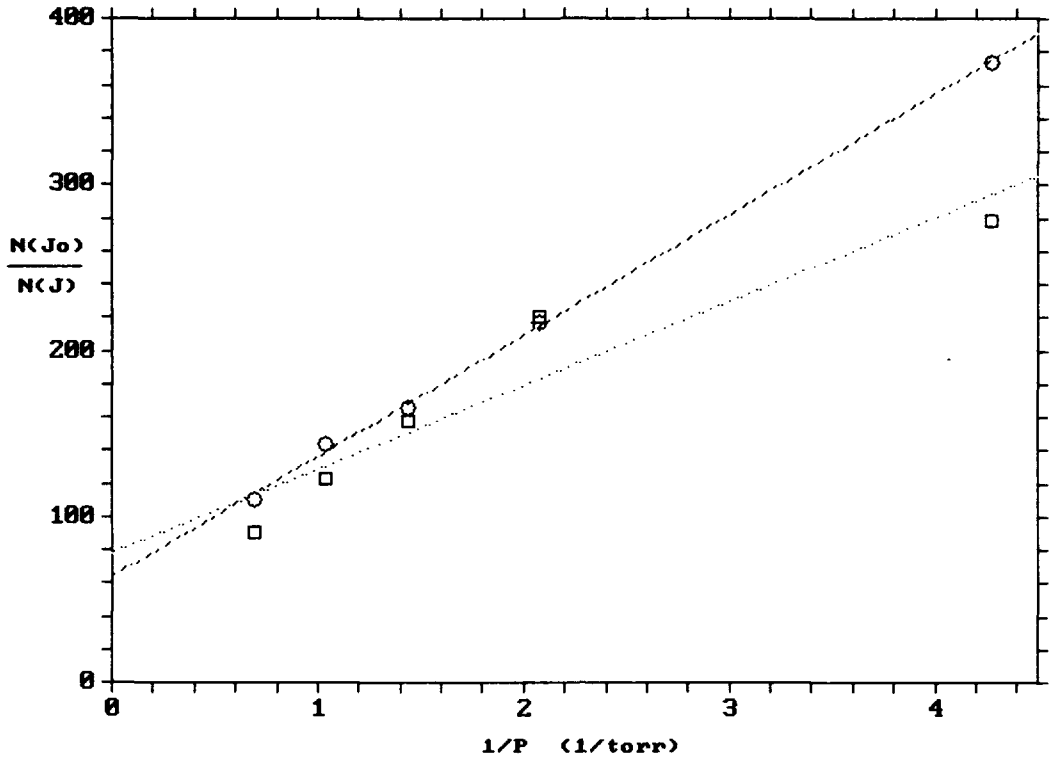

Figure 15. Stern-Volmer plot of bromine self quenching for Jo=35 -> J=41. Plot compares measured peak data vs area data for computation of population ratios. Upper curve is fit to peak height data; lower curve to area data.

Figures 14 and 15 depict representative bromine self transfer cases. Use of peak height values to calculate population ratios yielded more consistent results in Stern-Volmer plots than use of area measurements. This was expected for several reasons. The "peak height" measurements were adjusted for signal noise (measured from "floating baseline") while "area" measurements were not. The amount of signal noise experienced varied across each emission spectrum. Area measurements were also manually measured, not digitally integrated. Area measurements therefore yielded greater uncertainties in population ratios.

As noted in earlier discussion on how peak heights were measured, some values contained more "uncertainty" than others. To partially compensate for this, bromine self transfer plots were fit using a weighted linear regression routine. Data points with smaller uncertainties with respect to their population ratios were weighted more heavily. The larger uncertainties were generally associated with measured peak heights associated with large negative $\Delta J = J_f - J_i$.

3.2 Inert Gas Collision Partners

Following analysis of the self-transfer case, rotational energy transfer of the same exited bromine state was examined with different collision partners; He, Ne and Ar. Numerous spectra were generated for these cases with Br_2 pressures of 25 to 30 mTorr and bath gas pressures ranging from 100 to 2500 mTorr. In each of these cases, total removal rates were calculated by the same method described in the self transfer case. Individual state-to-state rotational rate constants were calculated by application of the nonlinear Stern-Volmer technique discussed earlier.

3.2.1 Helium

Six emission spectra for $Br_2(B:v'=11,J'=35)$-He rotational energy transfer were examined. Bromine pressure was maintained at 29.4 mTorr while Helium pressure ranged from 150 to 940 mTorr. Rotational lines were observed from $19 < J < 47$.

Total resolved fluorescence measurements were used to calculate the total rotational removal rate by the same means described for the self transfer case.

Convolved state-to-state rotational rate coefficients were calculated by means of the nonlinear Stern-Volmer technique

outlined earlier. A nonlinear, least squares fitting program was used to fit data in Stern-Volmer plots. Results are tabulated in the Results section.

3.2.2 Xenon

Six emission spectra for $Br_2(B:v'=11,J'=35)$-Xe rotational energy transfer were examined. Bromine pressure was maintained at 28 mTorr while Xe pressures ranged from 95 to 990 mTorr. Rotational lines were observed from $19 < J < 43$.

Total resolved fluorescence measurements were used to calculate a total rotational removal rate by the same means described in the self transfer case.

Convolved state-to-state rate coefficients were calculated by means of the nonlinear Stern-Volmer technique. Results are tabulated in the Results section.

3.2.3 Argon

Nine emission spectra for $Br_2(B:v'=11,J'=35)$-Ar rotational energy transfer were examined. Bromine pressure was maintained at 26 mTorr while Ar pressures ranged from 0 to 2.42 Torr. Emission lines were observed for $15 < J < 47$.

Total and state-to-state rotational rate coefficients were again calculated by the same means as for He and Xe. As would be expected for the higher pressures in these runs, these Stern-Volmer plots experienced significant nonlinear behavior.

Convolved state-to-state rotational rate coefficients derived from these plots are tabulated in the Results section.

3.3 Argon: Varied Parent States

In order to examine the behavior of rotational energy transfer with respect to J, two different rotational energy levels within the same vibrational band were populated. In addition to the $Br_2(B:v'=11,J'=35)$ parent level discussed in

the previous section, emission spectra for parent states of Br_2(B:v'=11,J'=26) and Br_2(B:v'=11,J'=47) with an Ar buffer gas were examined.

These three different sets of Br_2-Ar emission spectra were obtained at room temperature, approximately T=300° K. As shown in figure 16, for this temperature and vibrational band, the maximum "thermal" population resides at J=44. The three different bromine parent states selected (J' = 26, 35 and 47) represent states above, near and below this thermal maximum.

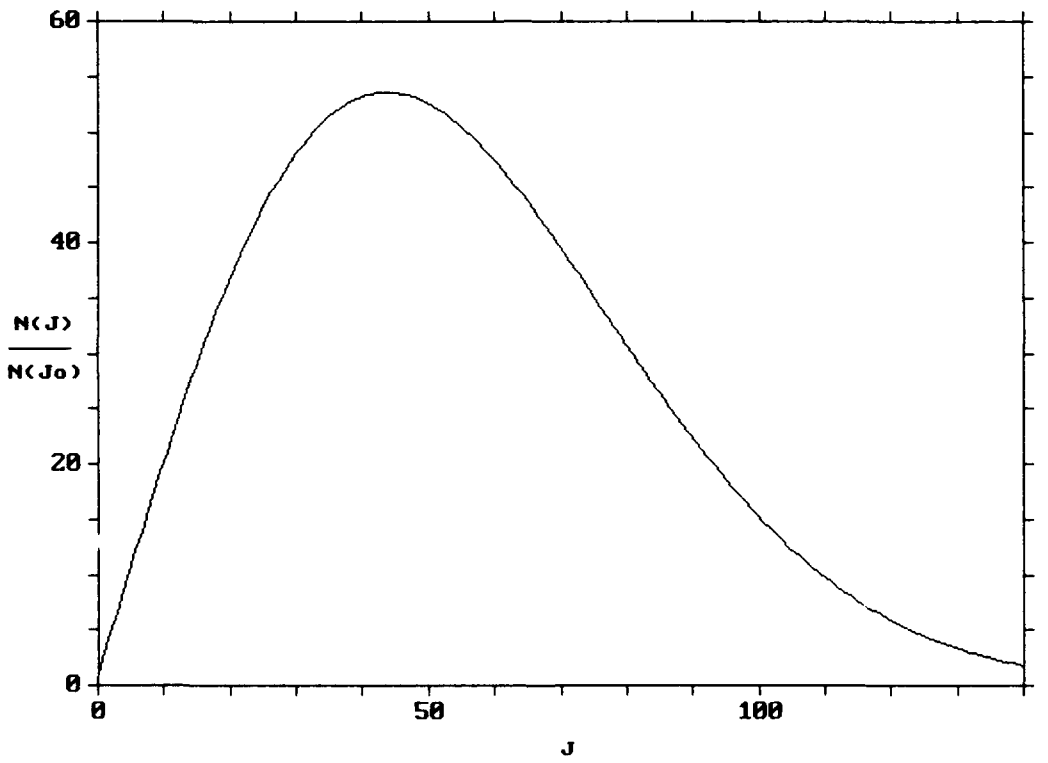

Figure 16. "Thermal" rotational population distribution for Br_2(B), v'=11, at T=300° K, based on boltzmann statistics. Boltzmann population maximum -> J = 44. Population distribution determined by $N_J/N_0 = (2J+1)e^{-BJ(J+1)/kT}$. (10:118)

In order to examine the behavior of rotational energy transfer with respect to vibrational band, another set of emission spectra was generated in which the pumped parent state was Br_2(B:v'=14,J'=36) with an Ar buffer gas.

3.3.1 Different Rotational Parent States

Six emission spectra were examined for Br2(B:v'=11,J'=47) parent state with an Ar buffer gas. Bromine pressure was maintained at 27 mTorr while Ar pressures ranged from 0 to 992 mTorr. Emission lines were observed for 25 < J < 55. Total removal and state-to-state transfer rate coefficients were calculated by means of nonlinear Stern-Volmer techniques. Results are tabulated in the Results section.

Five different emission spectra were examined for Br2(B:v'=11,J'=26) with an Ar buffer gas. Bromine pressure was maintained at 29 mTorr while Ar pressures ranged from 0 to 977 mTorr. Emission lines were observed for 14 < J < 40. Rate coefficients were calculated by means of nonlinear Stern-Volmer techniques and are tabulated in Results section.

Six emission spectra were examined for Br2(B:v'=14,J'=36) parent state with an Ar buffer gas. Bromine pressure was maintained at 25 mTorr while Ar pressures ranged from 0 to 990 mTorr. Emission lines were observed for 12 < J < 48. Rate coefficients were calculated by means of nonlinear Stern-Volmer techniques and are tabulated in the Results section.

3.4 Deconvolution

From the techniques applied in the previous sections, rotational rate constants were obtained for each of the cases noted. As noted earlier, these rate constants are convolved due to the P-R doublet overlap. The observed intensity of a

given emission line is proportional to both N(J) and N(J+6), the population densities of the parent states for the P-branch emission and R-branch emission. The observed intensity is defined by the relation

$$I(J+1) = N(J)S_P(J) + N(J+6)S_R(J+6) \tag{47}$$

where S_P and S_R are the J dependent line intensity functions for P and R branch emissions. They are defined as (12:208)

$$S_P(J) = \frac{J+1}{2J+1} \quad \text{and} \quad S_R(J) = \frac{J}{2J+1}$$

Thus far we have ignored the intensity variations of the P and R branch emissions which, as the relations above indicate, are a function of J. The following procedure to deconvolve calculated rate coefficients allows us to incorporate these line strength factors.

To deconvolve these rate coefficients, a scaling law that may apply to the cases investigated is selected. Various energy based and momentum based scaling laws have been applied to previous laser induced fluorescence studies of I_2, IF, and BrCl with the same collision partners under similar conditions. In each of these studies the exponential "Energy Gap Law" modeled the behavior of R-T rate coefficients for small changes in J ($\Delta J \leq 15$) to within 10%.

Rotational rate coefficients can be expressed in the form

$$K_{RT}(J_0 \rightarrow J_f) = K_c P_{J \rightarrow J'} \tag{48}$$

where Kc = the effective collision rate and $P_{J->J'}$ = the probability of R-T transfer per collision. The Polanyi-Woodall devised energy gap law (26:288), derived using semiclassical theory and Boltzmann gas-kinetic statistics, defines the probability of energy transfer per collision. This semiclassical approximation implies the probability of rotation-translation energy transfer is related to the "energy gap" between initial and final states by the relation

$$P_{J \rightarrow J'} = \alpha e^{-c|\Delta E|}$$

where a = an unimportant scaling constant and

$$\Delta E = B_v [J(J+1) - J_0(J_0+1)] \tag{49}$$

Using this energy gap law, the general expression for the rotational rate coefficient becomes

$$K_{RT}(J \rightarrow J') = K_c \{\alpha e^{-c|\Delta E|}\} = N e^{-c|\Delta E|} \tag{50}$$

where N = a new constant. Substituting for ΔE and using the value Jo (Jo = 35), we can define the equation describing the convolved rate constants as

$$K_{RT}^{Con} = \sum P(J) e^{-cB_v[J(J+1)-1260]} + \sum R(J) e^{-cB_v[(J+6)(J+7)-1260]}$$

where we define the functions

$$P(J)=\frac{S_P(J)}{S_P(J_0)} \quad \text{and} \quad R(J)=\frac{S_R(J+6)}{S_P(J_0)}$$

Equation (51) can be simplified to

$$K_{RT}^{Con}=Ne^{-cBv[J(J+1)-1260]}\{P(J)+R(J)e^{-cBv6(2J+7)}\} \tag{52}$$

The only unknowns in this equation are c and the scaling constant N. From equation (52), we define the part in brackets as F(J).

To deconvolve the rate calculated rate coefficients, the following iterative approach is applied:

1) Initially, let N'=NF(J), (assume F(J) is a constant) and plot K_{RT} vs J.

2) Fit $K_{RT}^{Con}=N'e^{-cBv[J(J+1)-1260]}$ to the plot from (1) and solve for c.

3) Using this value for c, calculate a value for F(J)

4) Using the value for F(J) above, calculate and plot the natural logarithm of K_{RT}/F(J) versus J.

5) Calculate a least squares fit to the plot from (4) above using the fitting function $K_{RT}^{Con}=\mathrm{Ln}[N]-cBv[J(J+1)-1260]$

6) From the fit in (5), use the new values for N and c to calculate a new value for F(J).

7) Repeat steps 4-6 until the values for c converge.

Once values for N and c are achieved, deconvolved rate are calculated using equation (50).

This procedure is applied separately for "uphill" (J_f-J_i>0) and "downhill" (J_f-J_i<0) transitions. Accordingly, different values for N and c are achieved for positive and negative values of ΔJ.

To test the assumption on whether the energy gap law applies to these cases, calculated values of N and c achieved by means described above were used in equation 52 to calculate "predicted" values for the convolved rate coefficients. If these predicted values match the measured values then the energy gap law may in fact apply for these cases studied. If they don't match within an acceptable error bound, then the energy gap law doesn't apply. This same general procedure could then be conducted utilizing other scaling laws.

Figure 17 depicts the results of this technique applied to the Br_2-He convolved rate coefficients. In this figure, the convolved rotational transfer rate coefficients, calculated as described earlier, are plotted with respect to J_f. The curves represent the "predicted" rates based on use of the energy gap law to deconvolve these rate coefficients. The close correlation between these two values indicates the energy gap law may apply for Br2-He rotational energy transfer (for $\Delta J < 20$).

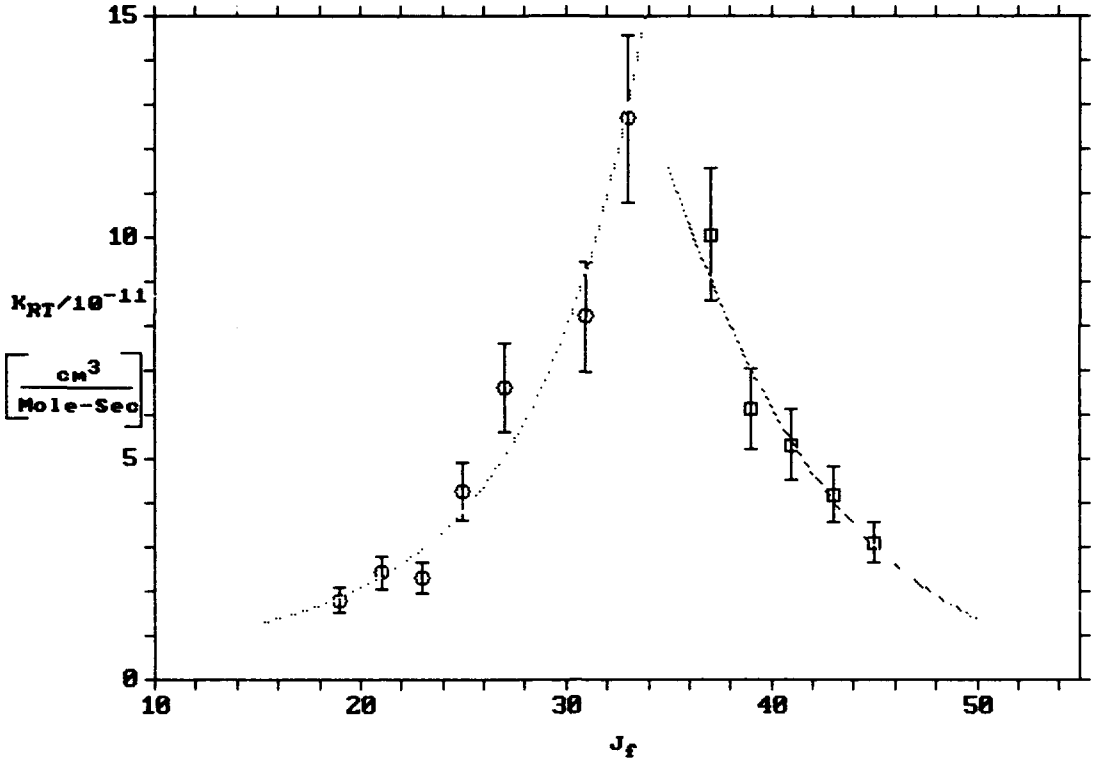

Figure 17. This figure depicts calculated convolved rotational rate coefficients for Br2(B:v'=11,J'=35) with He as collision partner. Curves depict "predicted" rates based on Energy Gap Law deconvolution routine. Close correlation indicates Energy Gap Law may be applicable for this case. Units of [cm^3/mol-sec]

This technique was used to deconvolve all the rotational rate coefficients for each case described. The closest correlation between measured and predicted convolved rate coefficients based on this approach was achieved for He as the collision partner. Figures 19 through 23 show the results of this deconvolution procedure for the remaining collision partners. The error bars for the convolved rates depicted in these figures correspond to the mathematical uncertainty generated in the Stern-Volmer analysis. Table II lists the values for "N"

and "c" achieved by this iterative technique. These values are used in equation 50 to determine the deconvolved rate coefficients listed in the next section as well as the "predicted" convolved rate coefficients depicted in Figures 18 through 23.

Table II. Fitting parameters for Energy Gap Scaling Law determined from iterative routine. (where $\Delta J = J_i - J_f$)

Case	N/10-11 [cm3/mole-sec]	C [cm]
Br_2(11,35)-Br2		
$+\Delta J$	1.341	0.0717
$-\Delta J$	3.1	0.0478
Br_2(11,35)-He		
$+\Delta J$	4.884	0.0363
$-\Delta J$	7.870	0.0253
Br_2(11,35)-Ar		
$+\Delta J$	3.834	0.0484
$-\Delta J$	7.706	0.0536
Br_2(11,35)-Xe		
$+\Delta J$	2.804	0.0562
$-\Delta J$	6.430	0.0559
Br_2(11,26)-Ar		
$+\Delta J$	3.251	0.0347
$-\Delta J$	6.000	0.0223
Br_2(11,47)-Ar		
$+\Delta J$	1.178	0.0261
$-\Delta J$	1.291	0.0112
Br_2(14,36)-Ar		
$+\Delta J$	23.71	0.0486
$-\Delta J$	32.95	0.0545

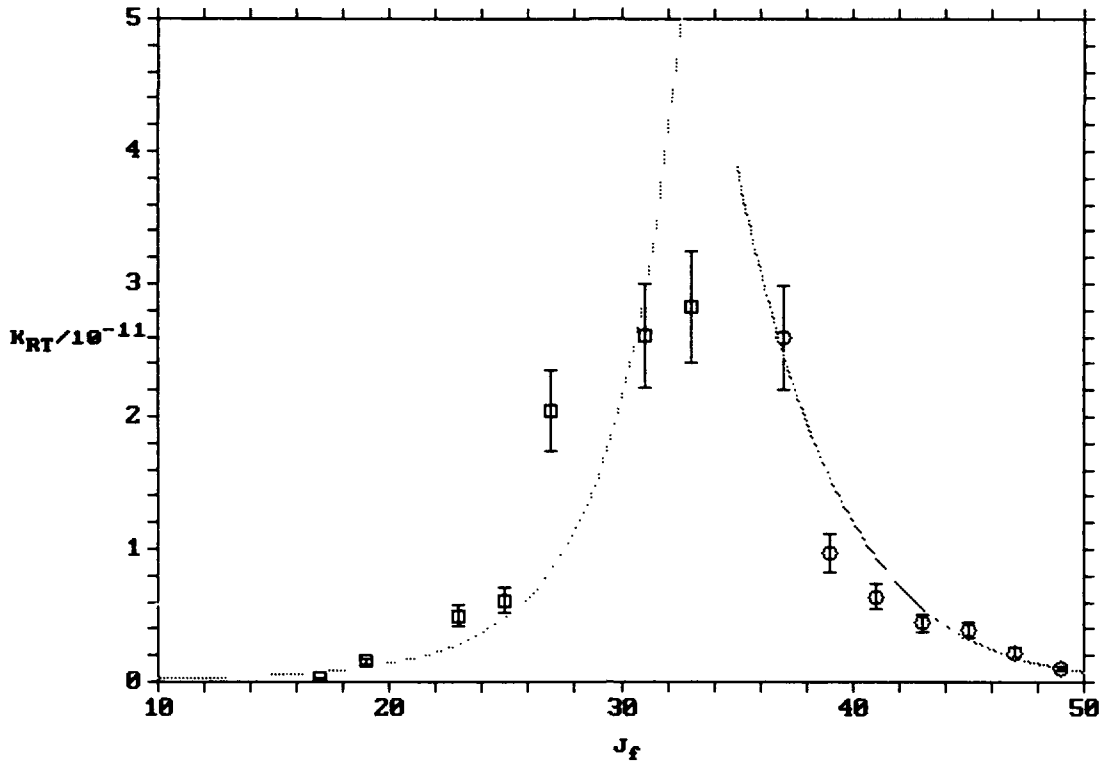

Figure 18. Br_2 self quenching case. Measured vs predicted convolved rotational rate coefficients based on Energy Gap Law deconvolution routine. Units of [cm^3/mole-sec].

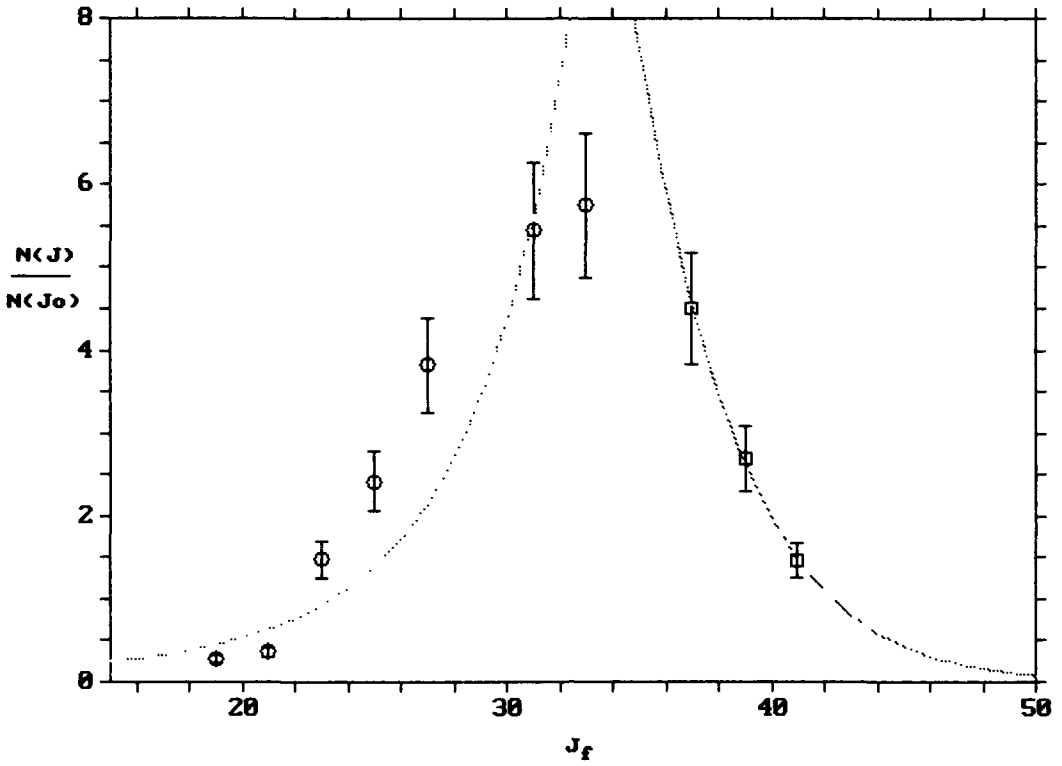

Figure 19. Measured vs Predicted convolved rotational rate coefficients for Br2(B:v'=11,J'=35) with Xe as buffer gas. Predicted rates based on energy gap law deconvolution routine. Units of [cm^3/mole-sec].

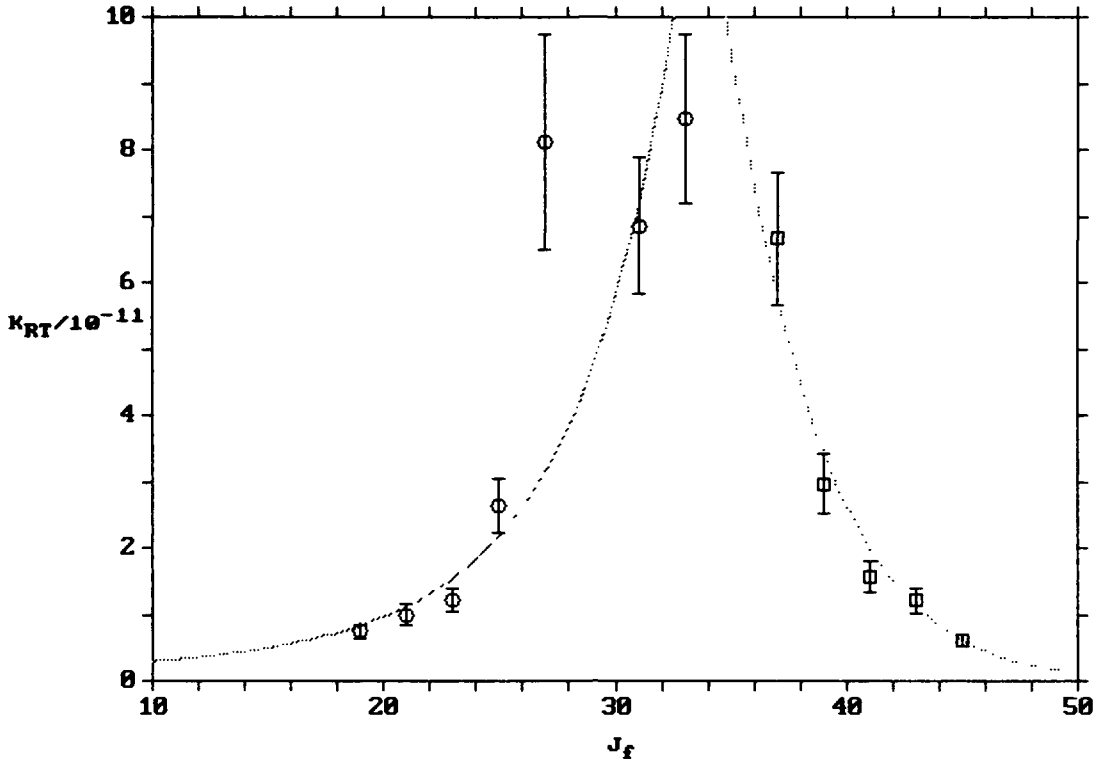

Figure 20. Measured vs Predicted convolved rotational rate coefficients for Br2(B:v'=11,J'=35) with Ar as buffer gas. Predicted rates based on energy gap law deconvolution routine. Units of [cm^3/mole-sec].

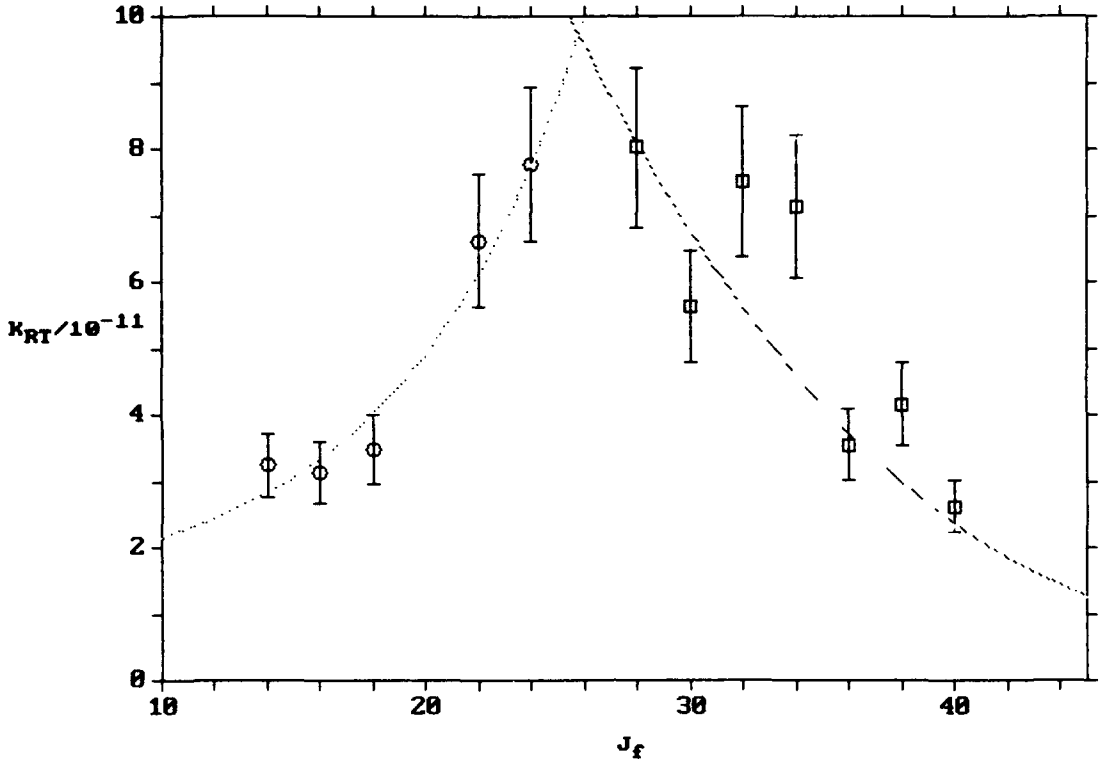

Figure 21. Measured vs Predicted convolved rotational rate coefficients for Br2(B:v'=11,J'=26) with Ar buffer gas. Predicted rates based on energy gap law deconvolution routine. Units of [cm^3/mole-sec].

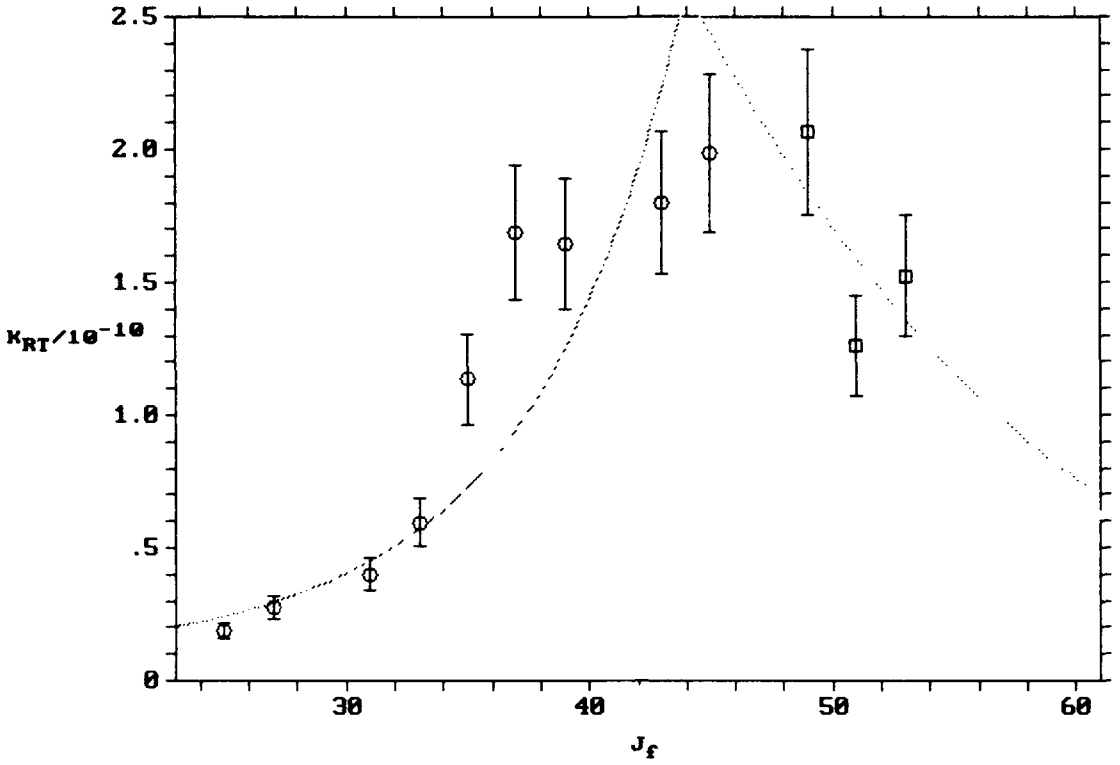

Figure 22. Measured vs Predicted convolved rotational rate coefficients for Br2(B:v'=11,J'=47) with Ar buffer gas. Predicted rates based on energy gap law deconvolution routine. Units of [cm^3/mole-sec].

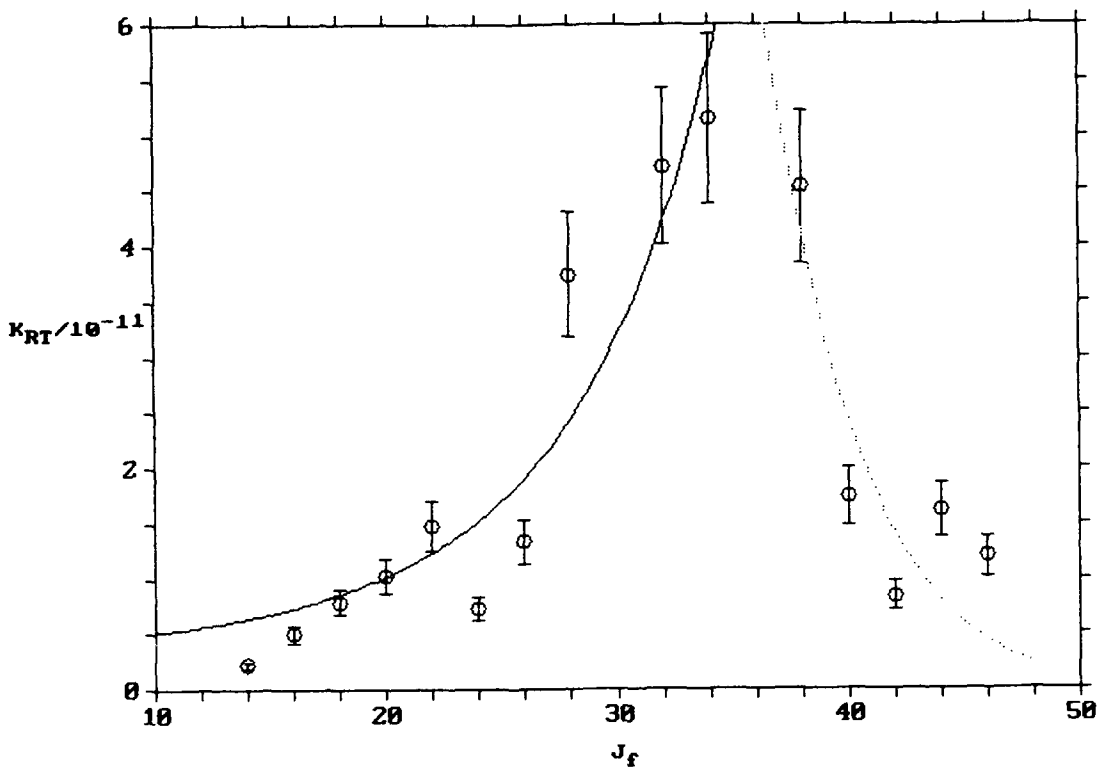

Figure 23. Measured vs Predicted convolved rotational rate coefficients for Br2(B:v'=14,J'=36) with Ar buffer gas. Predicted rates based on energy gap law deconvolution routine. Units of [cm^3/mole-sec].

An additional check supported the validity of this deconvolution technique. Using the values for "N" and "C" calculated through this iterative technique, rotational coefficients for $1 < J_f < 120$ were calculated using equation (50). For each of the Br_2(J'=35) cases, with Br_2(X), He, Ar and Xe collision partners, the sum of the these predicted state-to-state rotational rates matched the measured values for total rotational removal rates nearly exactly. For the other Br_2-Ar cases, the sum of state-to-state rates is within the error bound of the

measured total rotational removal rates. These close correlations lend credence to the applicability and accuracy of the energy gap scaling law for these cases.

3.5 Anomaly

In analyzing the numerous emission spectra in these various cases, a common "anomaly" was discovered. Depicted in Figure 24, the P(26) and P(22) emission lines on most of the spectra analyzed (for parent state Br2(B:v=11,J=35)) appear to have multiple peaks. These emission lines appear broader than their neighboring lines. This anomaly indicates the presence of a weak P-R doublet from another vibrational band of a different isotope of Br_2 (either $^{79}Br_2$ or $^{81}Br_2$). The implication is that the P(26) and P(22) emission lines are convolved not only with the R(30) and R(26) lines, but with a faint foreign P-R doublet as well.

The magnitude and precise origin of these foreign emission lines are unknown. Peak height measurements of the P(26) and P(22) lines, N(J=25) and N(J=21), were not corrected for this anomaly and likely to be too high. The corresponding convolved rate coefficients, for J_f = 25 and 21, are in turn expected too be too high. In examining Figures 17-21, for the Br2(v=11,J=35) parent state, the convolved rate coefficients corresponding to $21<J_f<25$ do indeed appear to be abnormally high with respect to their neighboring rate coefficients. Since the values for these convolved rates were used in the deconvolution process, this error is distributed among all the "downhill" deconvolved rate coefficients.

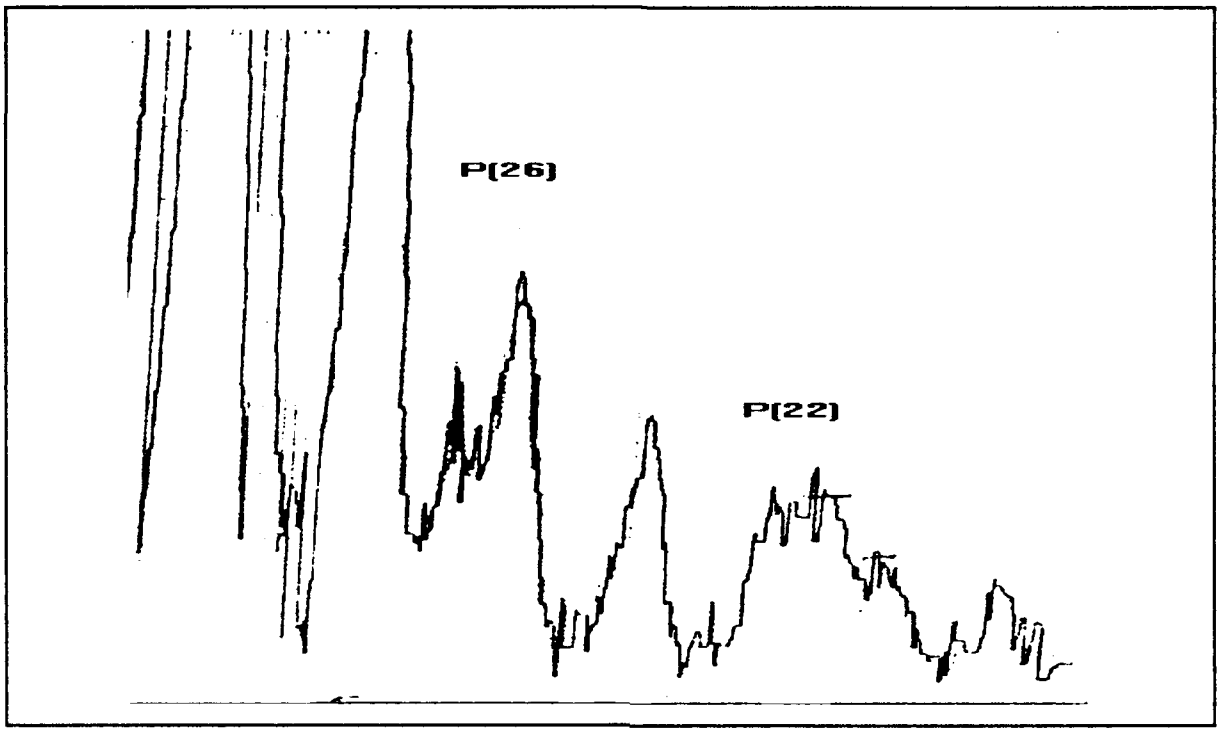

Figure 24. Portion of typical emission spectra from Br_2 LIF studies. The multiple peaks and broader width of the P(26) and P(22) emission lines indicate presence of P-R doublet, probably from another isotope of Br_2.

Part of the difference between the total removal rates calculated from total resolved fluorescence and total unresolved fluorescence may be attributed to this anomaly. The addition of a foreign emission would contribute to the total unresolved fluorescence making it slightly higher than it really is. However, the total resolved fluorescence of the J_1 emission lines were unaffected.

IV. Results and Discussion

Results of Stern-Volmer analysis on the cases discussed are tabulated in this section. Both convolved and deconvolved rate coefficients are given. Trends in data are discussed and comparison made with similar studies with other halogens and interhalogens.

4.1 Total Rotational Removal Rate Constants

Total rotational rate removal rates for each case examined are shown in Tables III and IV. The sum of state-to-state rotational rates for $1 < J_f < 120$ were calculated based on the energy gap law and the values of "N" and "c" derived in the iterative deconvolution process.

Table III. Total rotational removal rates calculated from linear Stern-Volmer analysis. The optically pumped parent state was Br_2(B:v'=11,J'=35). Values k^{RT}_{TOTAL} in units of $\left[\frac{cm^3}{Molecules-Sec}\right]$. First number is from total resolved fluorescence; second is summation of state to state rates; third is from total unresolved fluorescence.

Br2(B)-Br2(X)	Br2(B)-He	Br2(B)-Ar	Br2(B)-Xe
$(3.98 \pm 0.20) \times 10^{-10}$	$(5.8 \pm 0.6) \times 10^{-10}$	$(10 \pm 2) \times 10^{-10}$	$(6.6 \pm 0.6) \times 10^{-10}$
$\sum_{J_f} K_{ET}(J_i \rightarrow J) = 3.98 \times 10^{-10}$	$\sum_{J_f} K_{ET}(J_i \rightarrow J) = 5.8 \times 10^{-10}$	$\sum_{J_f} K_{ET}(J_i \rightarrow J) = 10 \times 10^{-10}$	$\sum_{J_f} K_{ET}(J_i \rightarrow J) = 6.6 \times 10^{-10}$
$(3.3 \pm 0.4) \times 10^{-10}$	-	-	-

Table IV. Total rotational removal rates for Br_2-Ar cases with varied parent states as determined from Stern-Volmer plots of total resolved fluorescence. Second term is summation of predicted state to state rates from $0 < J_f < 120$ based on energy gap law deconvolution routine. Values K^{RT}_{TOTAL} in units of $\left[\frac{cm^3}{Molecules-Sec}\right]$

Br2(B:v'=11,J'=26) -Ar	Br2(B:v'=11,J'=47) -Ar	Br2(B:v'=14,J'=36) -Ar
$(5.62 \pm 3)x10^{-10}$	$(5.67 \pm 2.3)x10^{-10}$	$(13.7 \pm 1.1)x10^{-10}$
$\sum_{J=1}^{120} k_{RT}(Jo \rightarrow J) = 4.3x10^{-10}$	$\sum_{J=1}^{120} k_{RT}(Jo \rightarrow J) = 1.14x10^{-10}$	$\sum_{J=1}^{120} k_{RT}(Jo \rightarrow J) = 12.9x10^{-10}$

The total rotational removal rate in the Br_2-Br_2 self quenching case of (3.98 +/- 0.55) x 10^{-10} is slightly lower than the lower bound rate of 4.4 x 10^{-10} calculated by Clyne, Heaven and Davis in their LIF studies of Br_2 (calculated from removal out of (14,4) state) . (4:975) In contrast to their bromine studies, this study found total rotational removal rates with collision partners He and Ar to be greater than that for $Br_2(X)$.

A common relationship examined with halogens in previous laser excitation studies has been scaling of the total rotational removal rate with the reduced mass of the collision partner. The R-T cross section is generally considered a more fundamental parameter than the rate coefficient. Though this study does not enable determination of true velocity dependent cross-sections we can calculate the effective "hard-sphere" cross sections, $\sigma(i \rightarrow f)$, using the relationship

$$\sigma_R(i \rightarrow f) = \frac{k_R(i \rightarrow f)}{\bar{v}} \qquad (53)$$

in which $\bar{v} = \left(\frac{8kT}{\pi\mu}\right)^{1/2}$

and μ is the reduced mass of the system. We can also express the ratio of the total R-T cross section to the effective hard sphere cross section, σ_R/σ_g. Classical arguments suggest that collision partners with larger mass may impart larger amounts of angular momentum to the rotating molecule upon collision. The ratio, σ_{RT}/σ_g, is directly proportional to the probability of rotational energy transfer. The systems angular momentum can be expressed, $L = \mu\bar{v}b$ where b = impact parameter. If rotational energy transfer is dependent on transfer of angular momemtum then this dependence will observed if the ratio σ_R/σ_g is proportional with the square root of the reduced mass of the system, $\mu^{1/2}$. Steinfeld and Klemperer present this argument in their I_2 studies and this angular momentum dependent relationship has been seen in I_2, IF and BrCl.

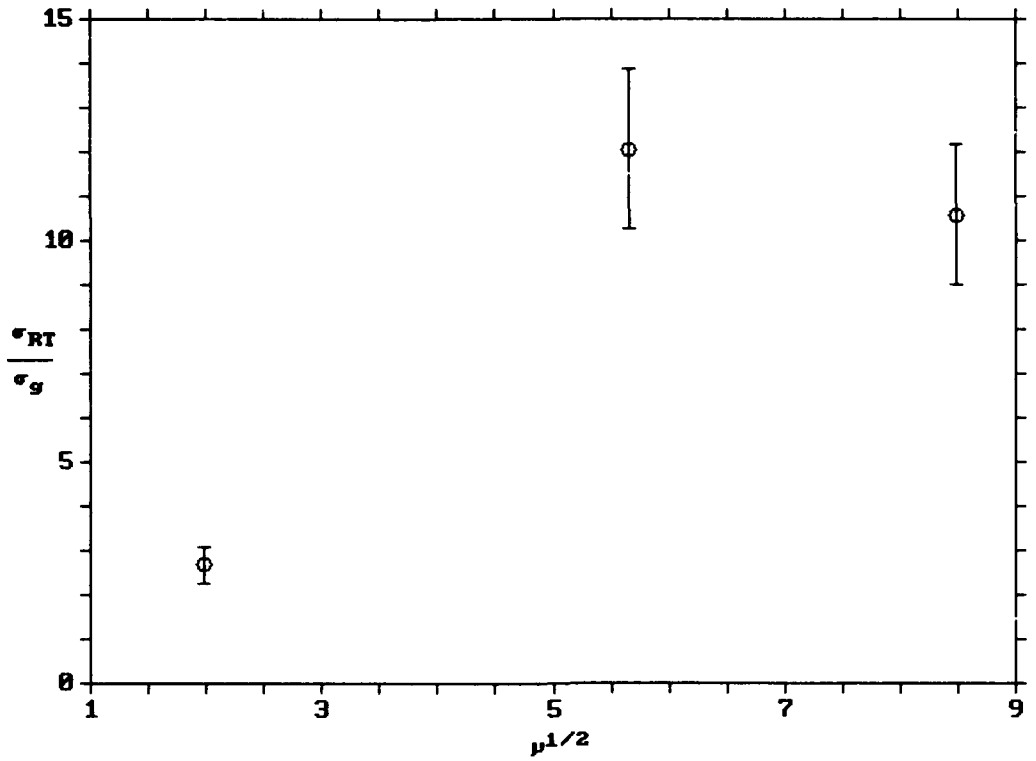

Figure 25. Scaling or total rotational removal rates from Br_2(B:11,35) with reduced mass of collision partner. Ratio σ_R/σ_g increased with reduced mass but not linearly.

Figure 25 depicts the reduced mass scaling results for Br_2. The ratio σ_R/σ_g increases with reduced mass. However, this relationship is clearly not linear. Given the error associated with the total removal rates calculated in this study, no conclusion can be reached in interpretating Figure 25.

4.2 Convolved Rotational Rate Constants

Convolved state-to-state rotational transfer rate coefficients for each case are shown in Tables V and VI. These rates were calculated from linear and nonlinear Stern-Volmer techniques described in sections 2 and 3. The errors asso-

ciated with all rate coefficients shown is +/- 30%. A more detailed discussion of estimated error limits is provided in Appendix B.

It is difficult to draw conclusions from examination of the rates presented in Table V because they are convolved. However, one can see a propensity for rotational energy transfer toward higher J levels. This propensity becomes more clear and is discussed further in the discussion of the deconvolved rate coefficients.

Table V. Convolved state-to-state rotational rate coefficients out of Br_2(B:11,35) state with various collision partners with respect to $\Delta J = J_f - J_i$. Error bound is +/- 30% for all values shown. (*) Unable to calculate convolved rate for this transition due to P(Jo) and R(Jo+4) overlap.

	$k_{RT} x 10^{-11}$ in units of $\left[\frac{cm^3}{Molecule-Sec}\right]$			
ΔJ	Br2(X)	He	Ar	Xe
-20	-	-	-	-
-18	0.02	-	-	-
-16	0.16	1.8	0.74	0.28
-14	1.9	2.4	1.0	0.37
-12	4.9	2.3	1.2	1.48
-10	4.8	4.3	2.6	2.42
-8	2.5	6.6	8.1	3.82
-6	*	*	*	*
-4	2.6	8.2	6.9	5.44
-2	2.8	12.7	8.4	5.74
2	2.6	10.1	6.7	4.5
4	0.98	6.1	3.0	2.69
6	0.64	5.3	1.6	1.46
8	0.45	4.2	1.2	-
10	0.39	3.1	0.6	-
12	0.22	-	-	-
14	0.11	-	-	-
16	-	-	-	-
18	0.04	-	-	-

Table VI. Convolved state-to-state rate coefficients for Br_2(B)-Ar rotational energy transfer. Initial pump states (v',J') are as shown. Error bound for all values is +/- 30 %. (*) Could not calculate rate due to P(Jo) and R(Jo+4) overlap.

	$k_{RT} \times 10^{-11}$ in units of $\left[\frac{cm^3}{Molecules-Sec}\right]$		
ΔJ	(v'=11,J'=26)	(v'=11,J'=47)	(v'=14,J'=36)
-20	-	1.89	0.5
-18	-	2.75	0.8
-16	-	4.02	1.0
-14	-	5.96	1.5
-12	3.24	11.4	0.8
-10	3.2	16.9	1.3
-8	3.5	16.4	3.7
-6	*	*	*
-4	6.6	17.9	4.7
-2	7.8	19.8	5.1
2	8.0	20.7	4.5
4	5.6	12.6	1.7
6	7.5	15.2	0.9
8	7.2	-	1.6
10	3.6	-	1.2
12	4.2	-	-
14	2.6	-	-

$\times 10^{-1}$

Examination of the rates in Table VI reveal two characteristics. First, for transfer out of the (11,35) level, the rate coefficients are greater for transitions to higher J levels (toward J_f>35). This is more apparent in the Br2(11,26)-Ar case where rates are greater for J_f>26 than J_f<26. However, in the Br2(11,47)-Ar case, rates are greater for J_f<47. This behavior could suggest a desire to reestablish a thermal distribution where the boltzmann maximum J level at T=300°K is J=44. Second, as seen in other LIF studies, the average

state-to-state rotational rates increase with J level. In comparing the Br_2(v'=11)-Ar cases, the measured rates in general increase with Jo (26, 35 then 47).

4.3 Deconvolved Rotational Rate Constants

Deconvolution of the state-to-state rates tabulated in the last section were accomplished by assuming the "Energy Gap" scaling law applied for these cases. The accuracy of these rates then rests on the validity of this assumption. Three noted observations lend confidence that this assumption is valid for small ΔJ transitions. First, discussed in detail earlier, is the fact that these deconvolved rates closely reproduce the convolved rates observed when applying the energy gap law. Second, the predicted sum of rotational rates based on the energy gap law for $1 < J < 120$ match nearly exactly the measured total rotational removal rates for transfer out of the Br_2(B:11,35) state. Finally, all previous studies with halogens and interhalogens have shown the energy gap scaling law to accurately predict rotational rates for small ΔJ.

The rates in Table VII depict the same propensity as their convolved parents for rotational energy transfer toward the boltzmann maximum rotational level, J=44. It also appears that the heavier collision partners yield smaller rates for the same ΔJ. These relationships are apparent when examining plots of these rates versus ΔJ shown in figures 26 through 30.

Table VII. Deconvolved state-to-state rotational rate coefficients. Rates for transfer out of Br_2(B:11,35) state with collision partners shown. Error bounds are +/- 30 % for all rates.

$k_{RT} x 10^{-11}$ in units of $\left[\frac{cm^3}{Molecules - Sec}\right]$				
ΔJ	Br2(X)	He	Ar	Xe
-18	0.019		0.212	
-16	0.026	0.654	0.265	0.126
-14	0.037	0.788	0.34	0.167
-12	0.056	0.966	0.446	0.229
-10	0.086	1.205	0.6	0.323
-8	0.138	1.532	0.826	0.468
-6	0.23	1.983	1.165	0.698
-4	0.397	2.613	1.684	1.069
-2	0.71	3.507	2.493	1.684
2	2.006	6.193	4.715	3.843
4	1.268	4.856	2.82	2.247
6	0.782	3.759	1.642	1.278
8	0.471	2.874	0.931	0.706
10	0.277	2.17	0.514	
12	0.159	1.617	0.276	
14	0.089			
16	0.049			
18	0.026			

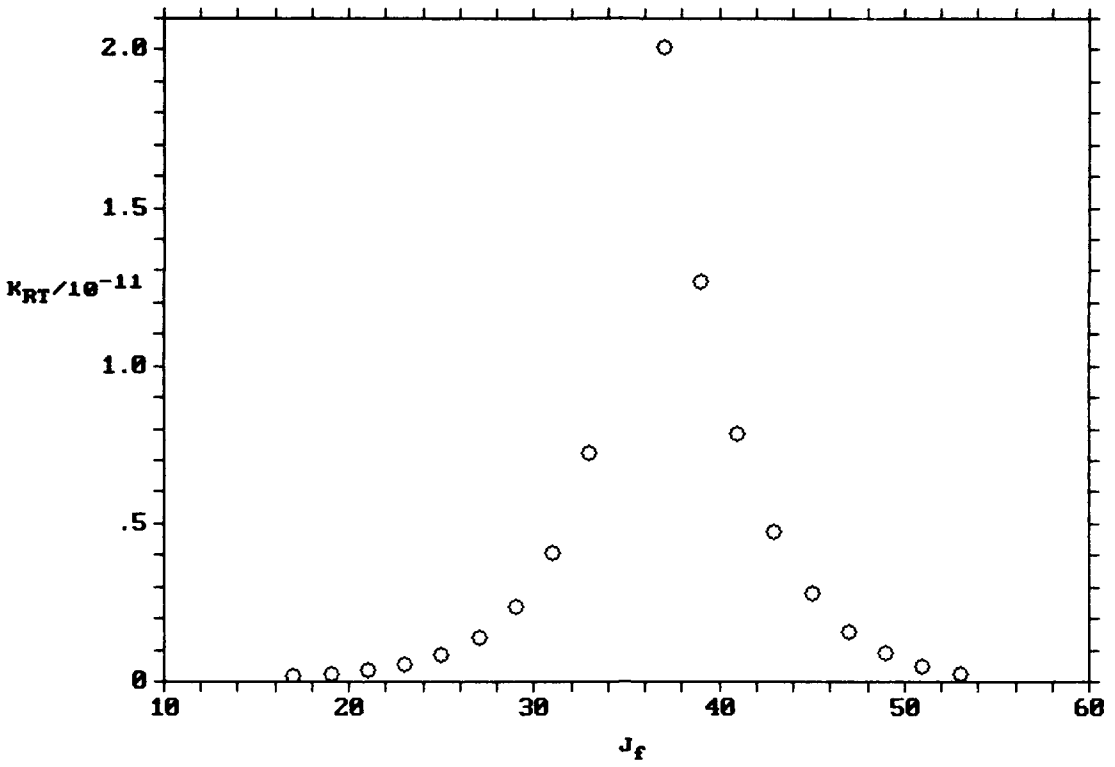

Figure 26. Br_2(B:11,35)-Br_2(X) Deconvolved rotational rate coefficients as a function of J_f.

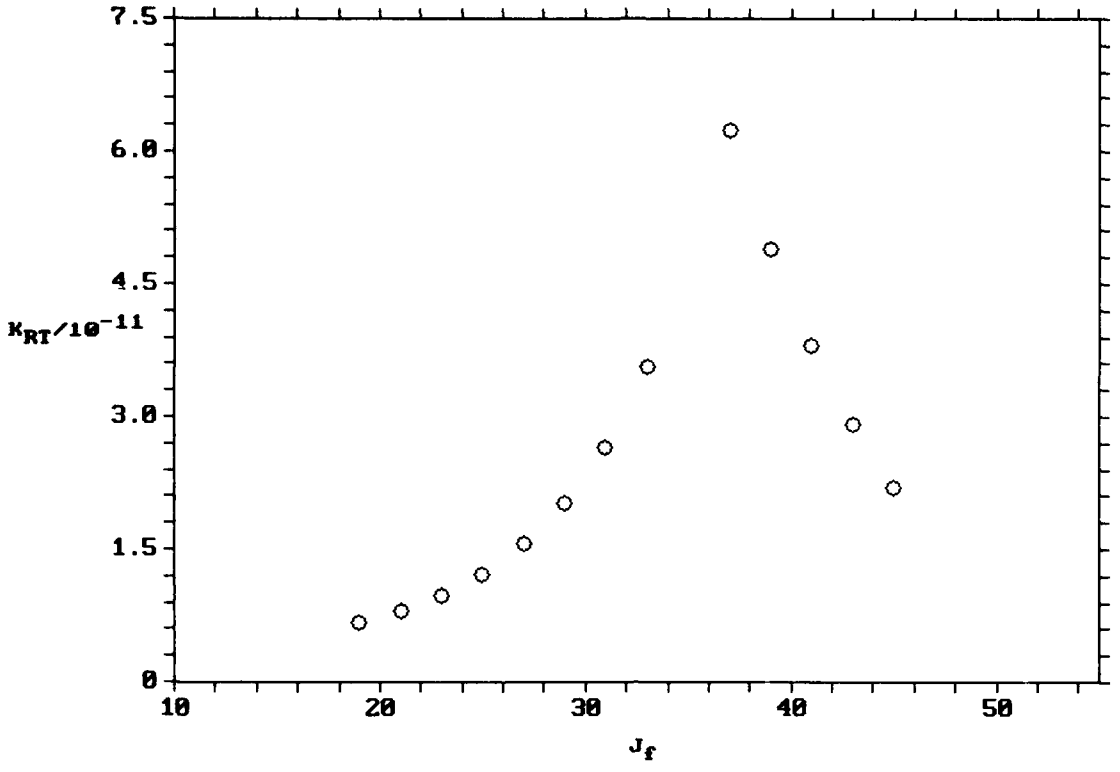

Figure 27. Br_2(B:11,35)··He Deconvolved rotational rate coefficients as a function of J_f.

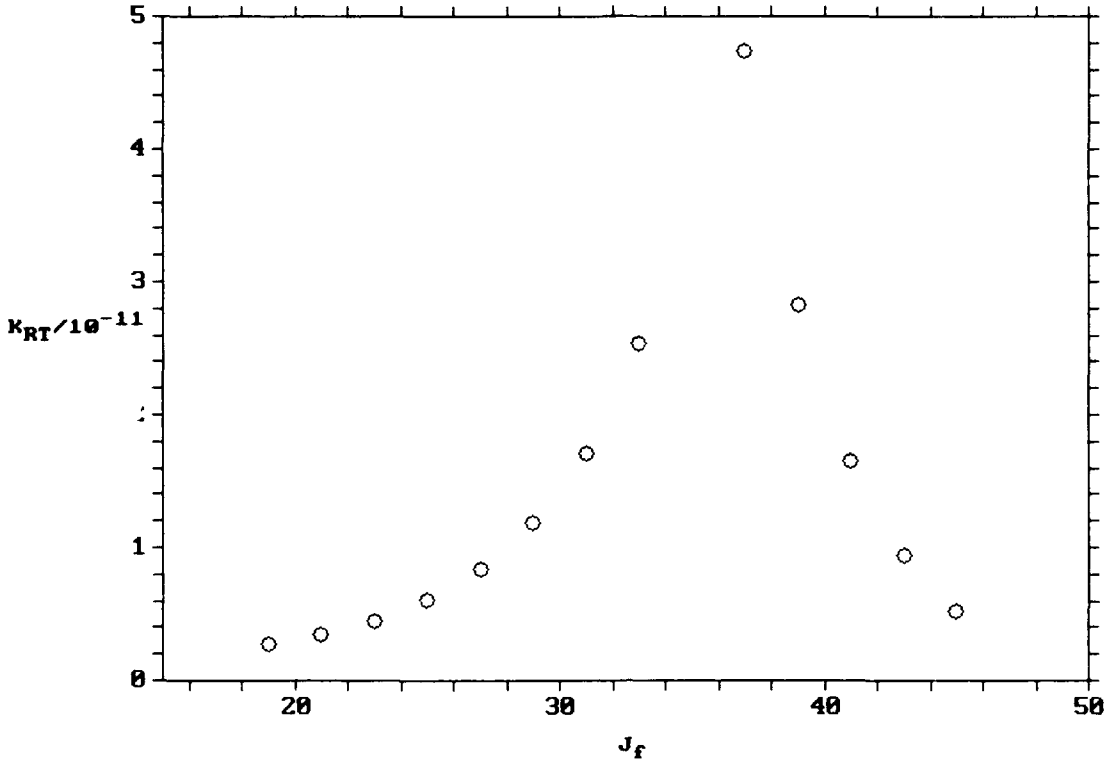

Figure 28. $Br_2(B:\,^3\Pi_{0_u^+},35)$-Ar Deconvolved rotational rate coefficients as a function of J_f.

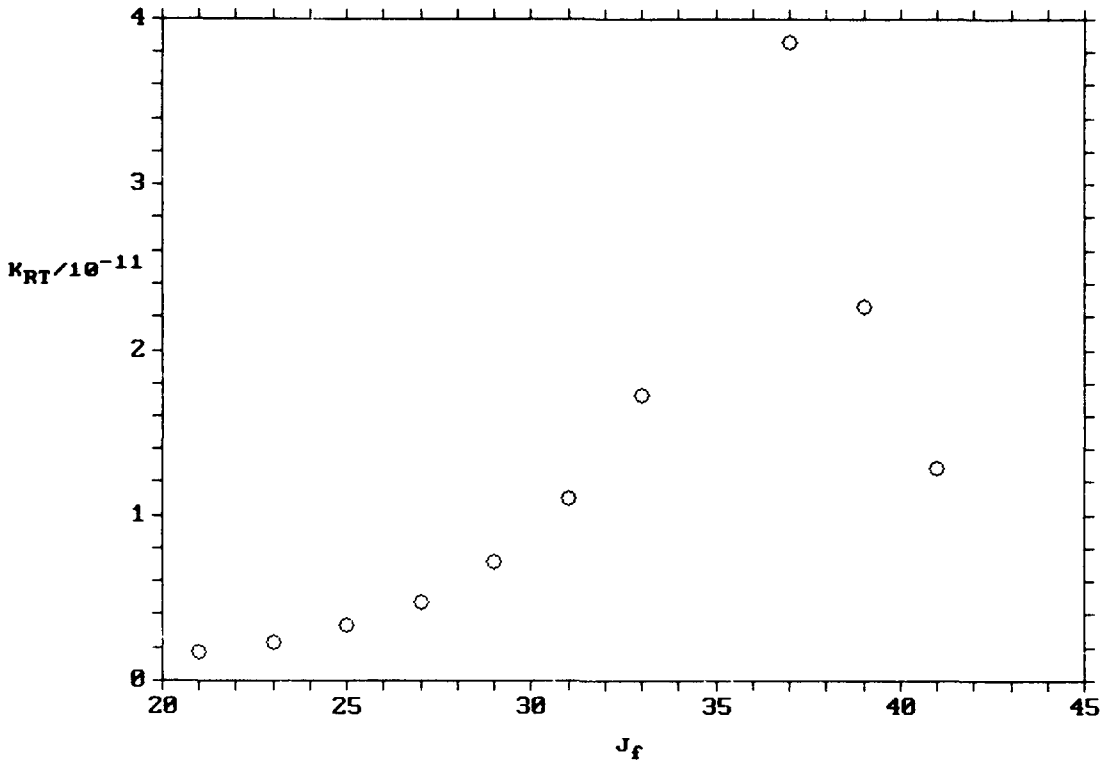

Figure 29. Br_2(B:11,35)-Xe Deconvolved rotational rate coefficients as a function of J_f.

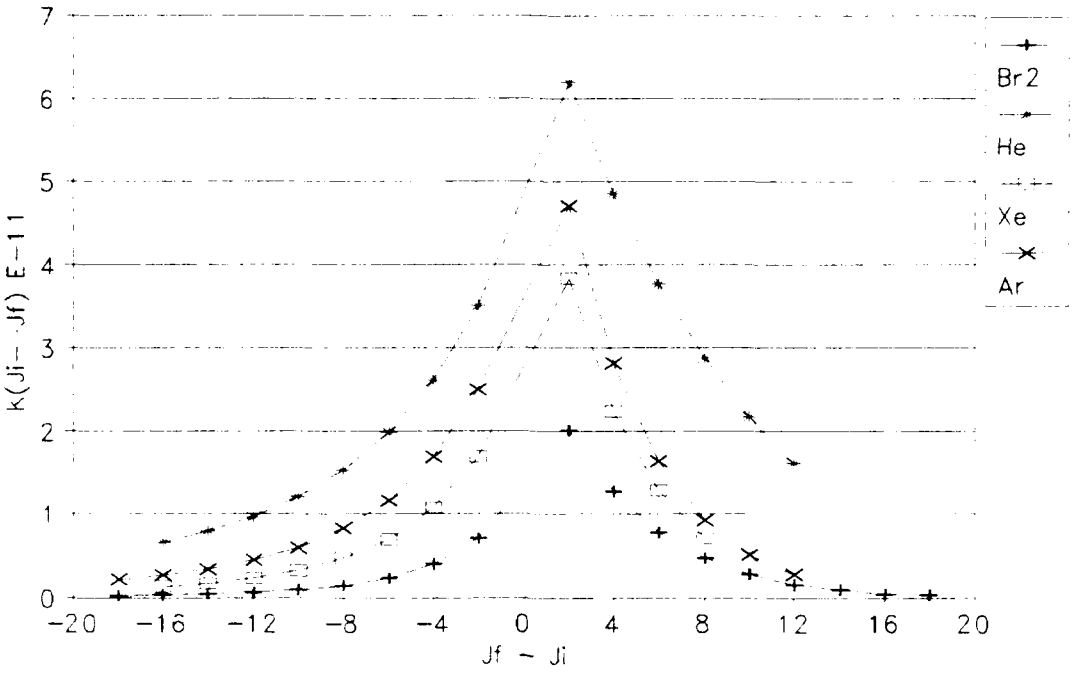

Figure 30. Br_2(11,35) Rotational rate coefficients for various collision partners as a function of ΔJ. Note that heavier collision partners yield smaller state-to-state rotational rates. Propensity for rotational energy transfer is toward boltzmann maximum, J=44.

A couple of distinguishable features can be discerned from these plots. First is the fall-off of $k_R(J_i \rightarrow J_f)$ with increasing ΔJ. This fall-off is clearly greater for He than for either Ar or Xe. In fact, this fall-off becomes less pronounced for heavier collision partners. This same behavior was observed in I_2 and IF studies. Second is the more pronounced fall-off for positive ΔJ or $J_f > J_i$. For J_i=35, a $\Delta J = +18$ upward energy transfer implies that the collision partner has supplied about 1 kT of energy (at T=300° K). One can logically assume that upward energy transfer for $\Delta J > 18$ is

probably energy limited. The sharper fall-off observed for upward energy transfer rates in these plots supports this assumption.

As shown for total removal rates earlier, another means of depicting these rates is in the form of velocity independent, hard sphere collisional cross sections. Figure 31 through 34 depict these same state-to-state rotational rate coefficients in the form of collision cross sections. This transformation assists in comparing these results with those for other halogens.

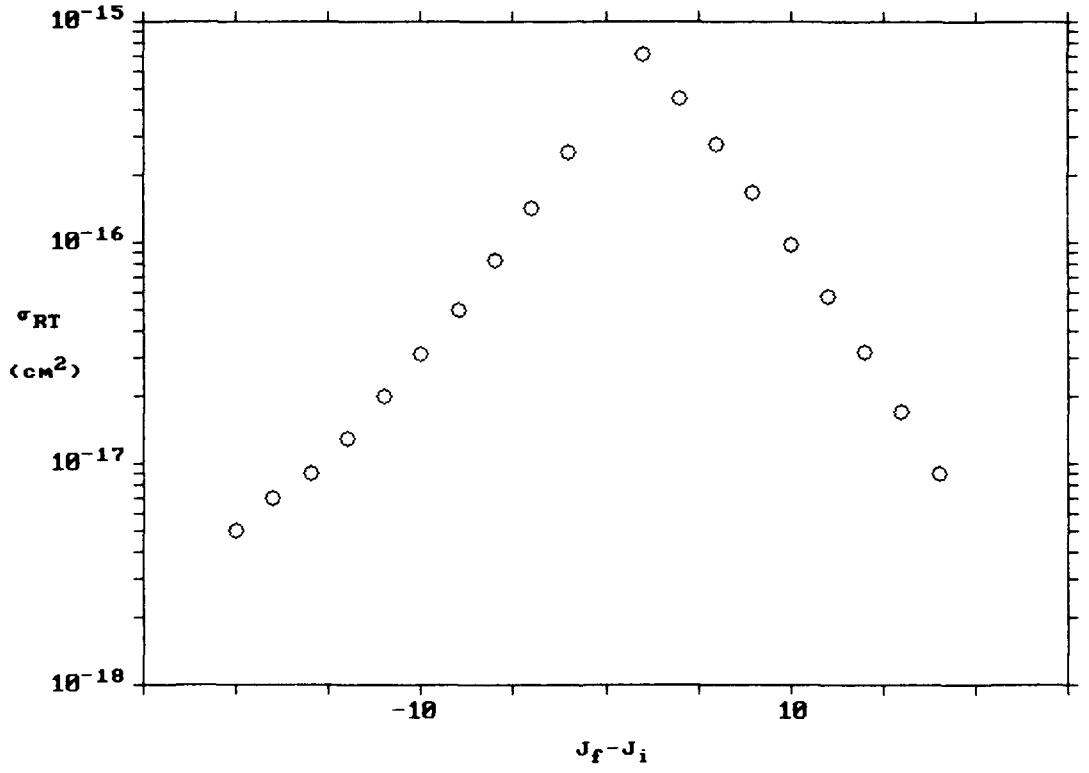

Figure 31. $Br_2(B)-Br_2(X)$ Rotational transfer velocity independent cross sections as a function of ΔJ.

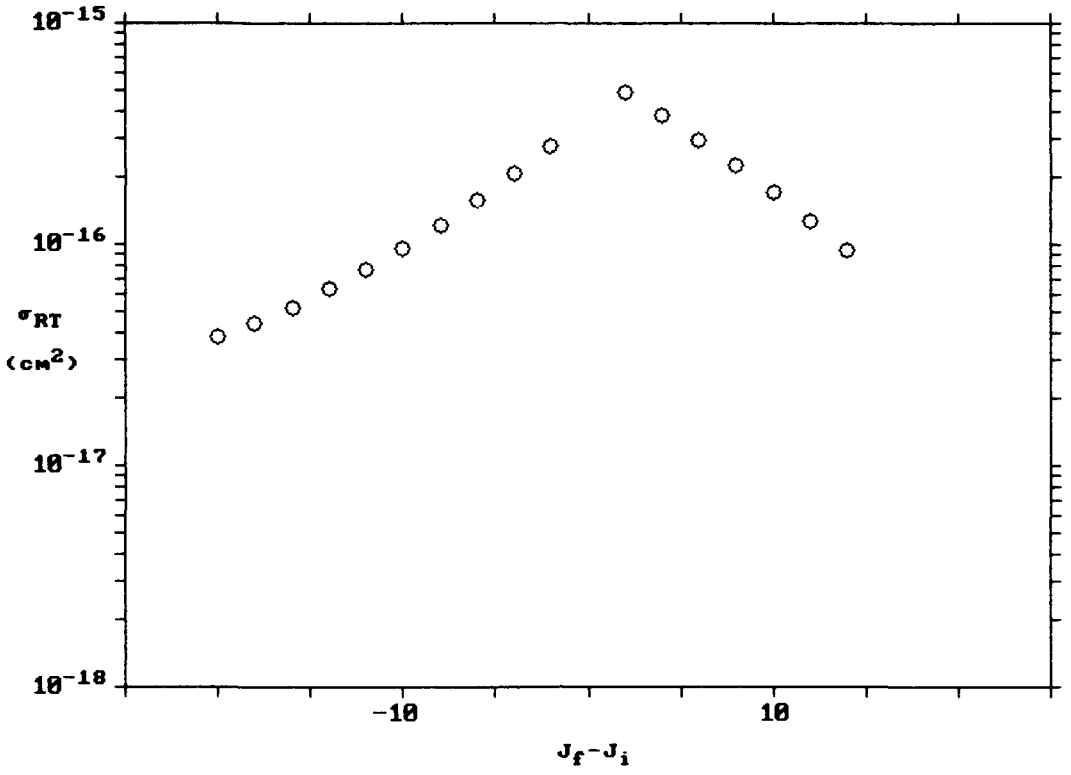

Figure 32. Br_2-He Rotational transfer velocity independent cross sections as a function of ΔJ.

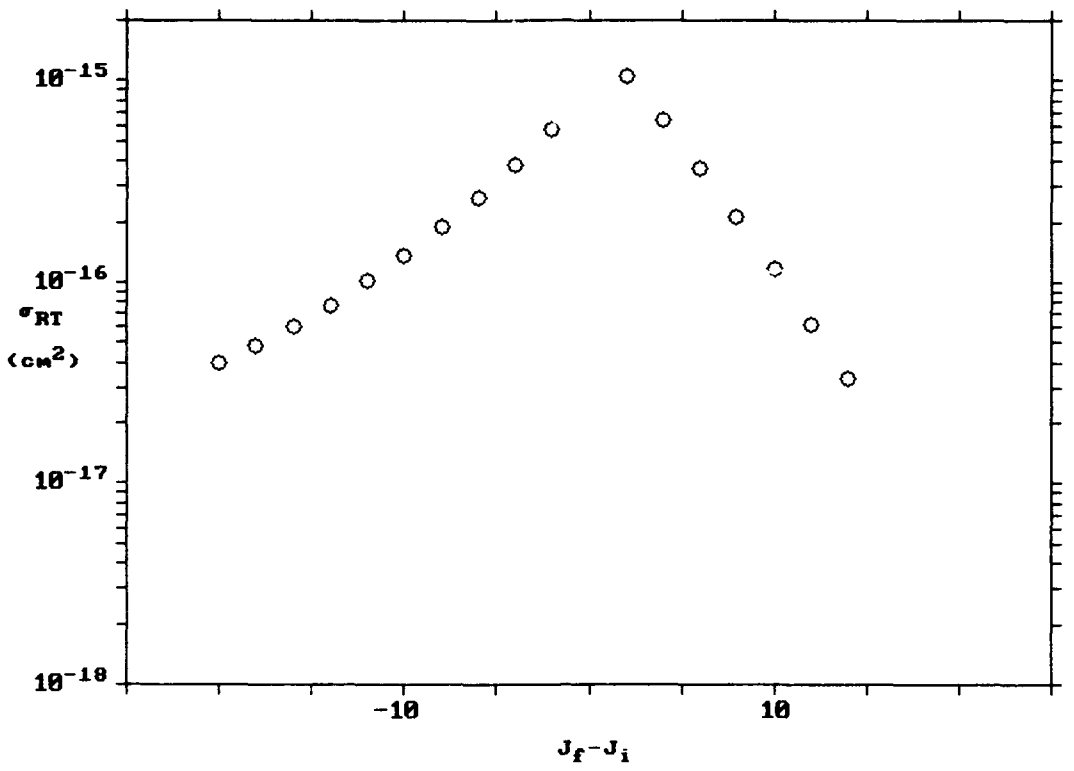

Figure 33. Br_2-Ar Rotational transfer velocity independent cross sections as a function of ΔJ.

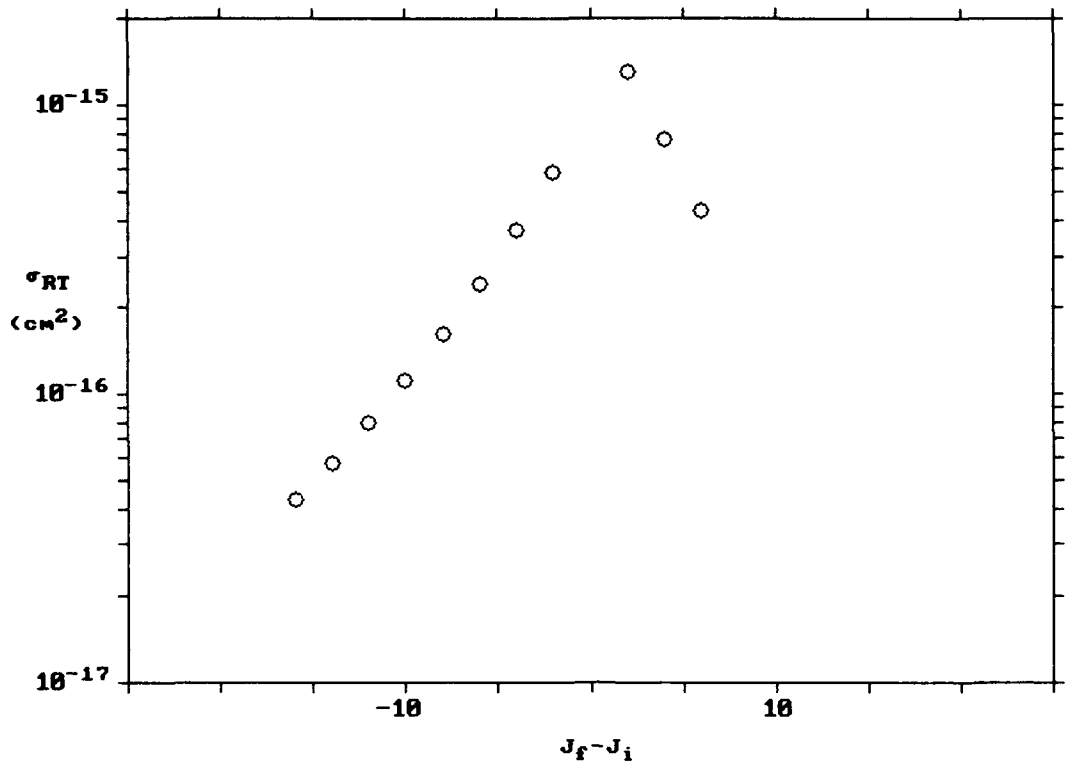

Figure 34. Br_2-Xe Rotational transfer velocity independent cross sections as a function of ΔJ.

Previous laser excitation studies of I_2 and IF demonstrated a "broadening" in plots of σ_R versus ΔJ as the mass of the collision partner increases. Figures 31 through 34 show the opposite for Br_2 where the plots narrow vs broaden for an increase in mass of collision partner.

Deconvolved rates for the other Br_2-Ar cases are listed in Table VIII and depicted in Figures 35 through 37 as a function of ΔJ. These figures (for Br_2(11,26)-Ar and Br_2(11,47)-Ar) clearly demonstrate the propensity for rotational energy transfer toward the boltzmann maximum, J=44.

Table VIII. Deconvolved state-to-state rotational rate coefficients as a function of ΔJ with Ar as a collision partner. Various different parent states of $Br_2(B)$ were examined. Specific (v',J') noted in table. Error bound is +/- 30%.

$k_{RT} x 10^{-11}$ in units of $\left[\frac{cm^3}{Molecules - Sec}\right]$			
ΔJ	(v'=11,J'=26)	(v'=11,J'=47)	(v'=14,J'=36)
	-	1.01	1.51
-20	-	1.22	1.76
-18	-	1.49	2.09
-16	-	1.84	2.53
-14	1.06	2.3	3.12
-12	1.21	2.91	3.93
-10	1.41	3.74	5.05
-8	1.67	4.87	6.62
-6	2.01	6.42	8.84
-4	2.46	8.58	12.05
-2	5.13	11.18	16.74
2	4.33	9.72	21.8
4	3.61	8.4	14.11
6	2.98	7.22	8.93
8	2.43	-	5.53
10	1.96	-	3.35
12	1.56	-	1.99
14			

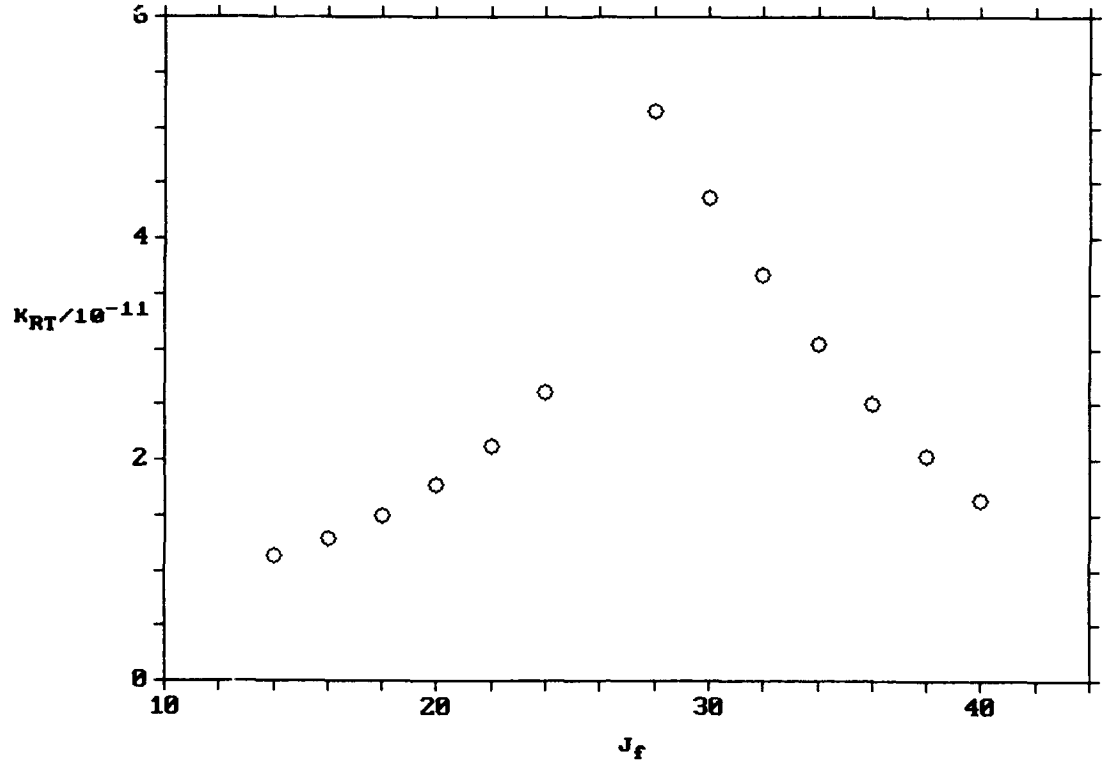

Figure 35. State-to-state rotational rate coefficients for Br_2(B:11,26) system with Ar as collision partner.

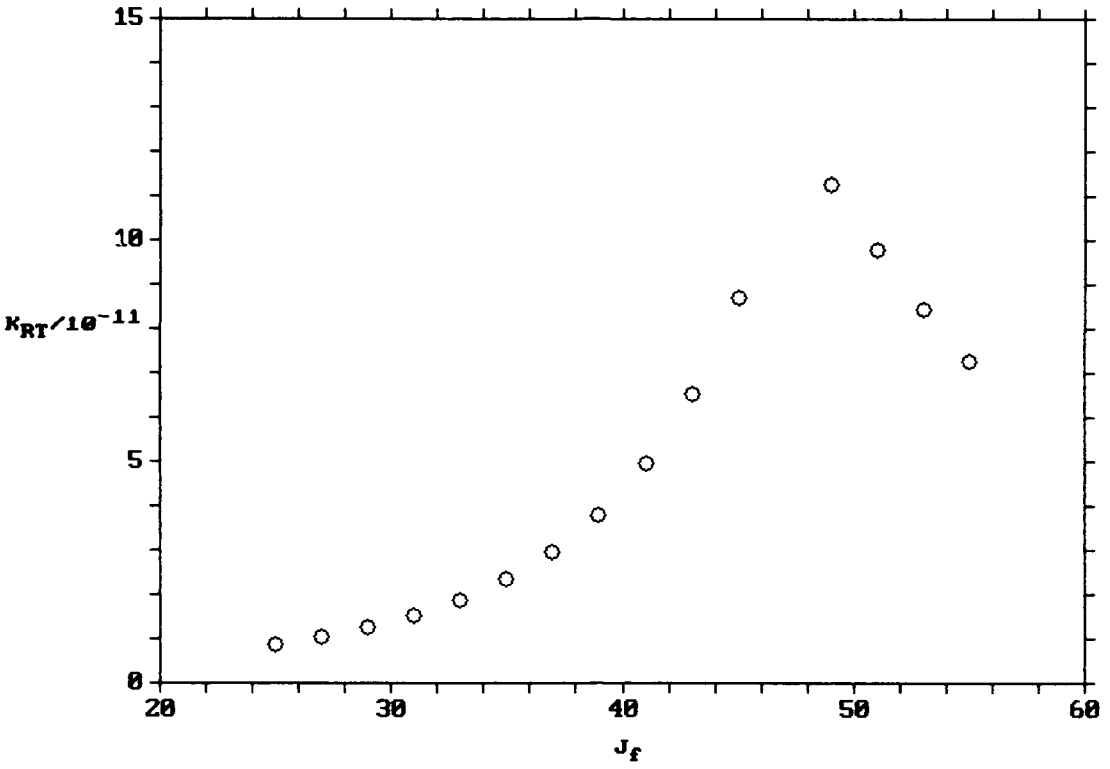

Figure 36. State-to-state rotational rate coefficients for $Br_2(B:11,47)$ system with Ar as collision partner.

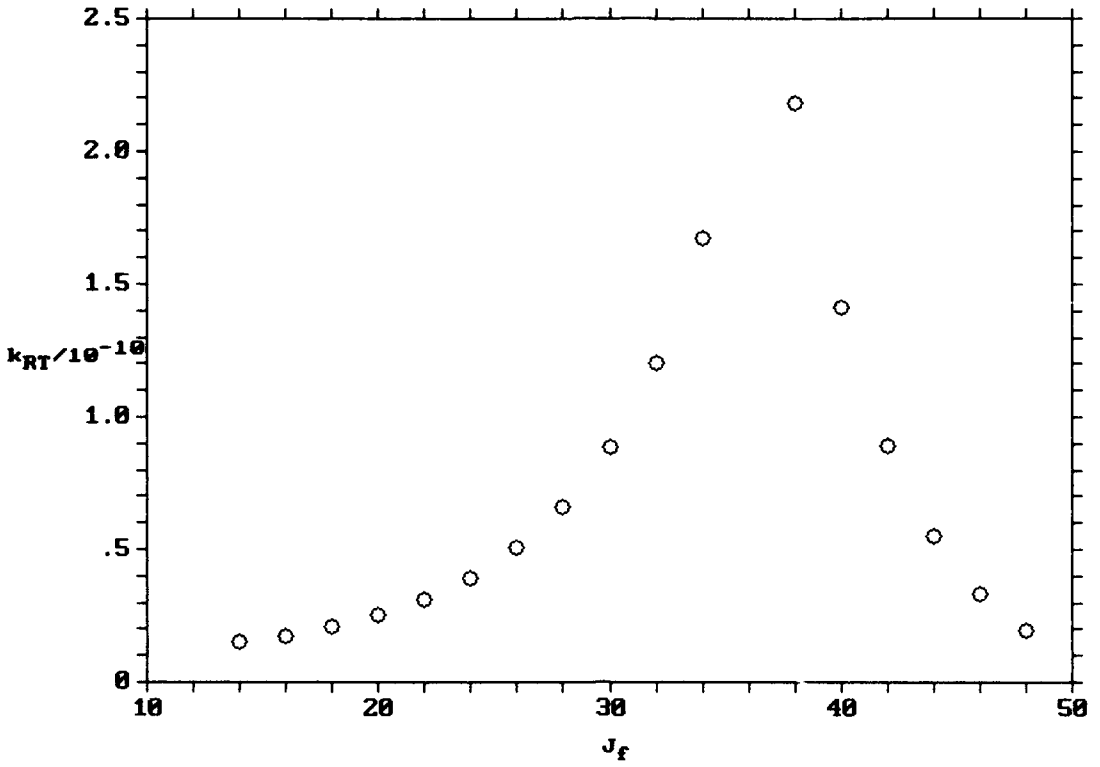

Figure 37. State-to-state rotational rate coefficients for Br_2(B:14,36) system with Ar as collision partner.

Several interesting features can be discerned from comparing the four different Br_2-Ar cases. The distribution of rotational rates for the J_i=35 case seems to be flatter than for the higher and lower J_i's within the same vibrational band. The state to state rates for J_i = 26 and 47 for small ΔJ are larger than for J_i = 35, yet the total rotational removal rate for J_i = 35 is larger than for the other two cases. The distribution of state-to-state rates for the (14,36) system is similar but more symmetric than either case within the v'=11 band. This is consistant with observations in the v' = 11 band since the boltzmann maximum for this vibrational band at T=300° k is J = 36, the initially excited state. The (14,36->J_f)

rates are somewhat larger for large ΔJ's. This result coincides with the larger total rotational removal rate measured for this case. This parallels previous halogen studies where rate coefficients become greater for higher vibrational bands.

As noted several times earlier, these cases serve well to demonstrate the propensity for rotational energy transfer toward the boltzmann maximum J level. The variance in the magnitude of the individual state-to-state rates as well as the total rotational removal rates in these separate cases may imply a J dependence for rotational energy transfer. No comparison can be made with these results and similar rotational transfer studies conducted with IF-Ar.

V. Conclusions

5.1 Discussion

In this study of the $Br_2(B)$ + $Br_2(X)$ system, a total rotational removal rate of $(3.98 \pm 0.2) x 10^{-10}$ $[cm^3/Molec-Sec]$ was determined. This rate is lower than that found in previous Br_2 studies (lower bound of $4.4x10^{-10}$ found by Heaven).

Rotational energy transfer with foreign collision partners was examined for several different optically excited parent states. State-to-state rotational removal rates with respect to ΔJ were found to decrease with increasing mass of the collision partner. A propensity for energy transfer toward the boltzmann maximum, J_{max}, was consistently observed for all cases. Plots of hard-sphere, velocity independent rotational cross sections, σ_R, with respect to ΔJ became "narrower" with increased mass of collision partner. This behavior is opposite to that seen in similar I_2 studies.

Deconvolution of state-to-state rate coefficients was performed by assuming a form of the scaling law, the exponential "Energy Gap Law". This scaling law adequately described rotational energy transfer in other halogen studies for small ΔJ, ($\Delta J < 20$, and appears to do the same for Br_2. The resultant parameters identified in this process yielded good fits to the data and closely reproduced the convolved rate coefficients. These same parameters in turn predicted the same total rotational removal rates as were measured in this study. These close correlations indicate that the "Energy Gap" scaling law may in fact describe the systems presented in this study. Other energy based and angular momentum based scaling laws were not examined in this study.

Variations in rate coefficients and total removal rates for different parent J levels may imply a J dependence on rotational energy transfer. State-to-state rates in general became larger for larger values of J. As with other halogen studies, total removal and state-to-state rate coefficients increased with higher vibrational levels.

The nonlinearity displayed in plots of σ_R/σ_q versus $\mu^{1/2}$ do not support an angular momentum dependence. This study also demonstrates a departure from other halogen studies regarding behavior of σ_{RI} with the mass of the collision partner. Given the error associated with this study, and failure to apply angular momentum based scaling laws to this data, no definite conclusion on J dependence can be reached.

5.2 Recommendations for Future Studies

5.2.1 Comparison of Scaling Laws

The deconvolution of rates in this study assumed use of only one possible scaling law, the "Energy Gap Law". In previous studies with I_2 and IF, the EGL produced fair results for small ΔJ but failed for larger ΔJ's. Since the predictive power of scaling laws is critical to any kinetics code that includes rotational energy transfer, it would be wise to apply other scaling laws to the convolved rates listed in this study. Several energy based and angular momentum based scaling laws have been applied to other halogen studies.

Pritchard and co-workers developed the "power Gap Law", an energy based scaling law that scaled R-T rate coefficients to the relation: (25:2115)

$$k(i \rightarrow f) = \alpha \left| \frac{\Delta E}{B_v} \right|^{-\sigma} N_\lambda(J_i, J_f)(R(\Delta E)) \qquad (54)$$

where α, σ, and λ are fitting parameters, B_v is the rotational constant, and N_λ is a factor that allows for a restriction on ΔM or a change in orientation of the molecule during the collision. While the exponential energy gap law can be derived from statistical principles, the validity of the power gap law rests primarily with with better fits to rotational energy transfer data. The power law generated good fits to I_2 and IF data.

Two angular momentum based scaling commonly applied are the "Infinite Order Sudden Law" and "Energy Corrected Sudden Law" (27:3329). These scaling laws have been successfully applied to a number of homonuclear molecules to include I_2. In IF studies, these scaling laws yielded results comparable to those from the power gap law.

Each of these scaling laws should be applied to the convolved rate coefficients tabulated in section 4. Deconvolved rates can be derived by means similar to that in this study. Comparisons can then be made on how well each scaling law predicts the distribution of convolved rates. Comparisons of predicted total rotational removal rates versus measured rates can also be made. Though this technique of deconvolving rate coefficients by assuming a form of the scaling law will not in itself identify which scaling law applies, it will identify which laws may apply. It can also eliminate laws that don't adequately reproduce the convolved rate data.

The constants and rotational rates derived from these investigations can also be combined with results from other bromine studies to generate a code to calculate theoretical spectral distributions for bromine under varying conditions. These computer generated spectral distributions can be compared with those recorded from various different bromine studies.

5.2.2 Future Br2 LIF Studies

Future laser induced fluorescence studies of $Br_2(B)$ will be required in order to fully examine the kinetics of vibrational and rotational energy transfer. The separate laser excitation studies of Br_2 by Clyne, Heaven and Perram have yet to reproduce matching results for rotational energy transfer. The problems experienced in this study prompt the following recommendations for future Br_2 LIF studies:

(1) Bromine operating pressures should be reduced to alleviate secondary effects. Given the strong predissociative nature of Br_2, the trade off will be lower emission intensities.

(2) Record digital emission spectra. Digitized spectra allow for more accurate measurements of "area" associated with specific emission lines. More accurate population ratios can be ascertained and utilized in the Stern-Volmer analysis. Corrections to emission spectra for noise and other effects can be effected more easily. Use of digitized spectra potentially eases making comparisons of computer generated spectra with recorded emission spectra. If nothing else, floppy disks are less bulky and easier to handle than stacks of X-Y plotter paper.

(3) Great care needs to be taken to reduce the noise generated in emission spectra. Scattering of the pump beam within the reaction chamber, as well as other outside light sources, can be reduced through prudent use of appropriate filters and detection equipment. This is especially important when operating at low bromine pressures where emission intensities are low.

(4) Specific absorption lines selected for optical excitation of $^{79}Br^{81}Br$ should be chosen carefully to insure that emission spectra generated are not corrupted by emissions from other Br_2 molecular isotopes.

Appendix A - Line Positions

An electronic spreadsheet created by G. Perram incorporating the spectroscopic constants listed in table I was used to generate predicted line positions for $Br_2(B)$ emission spectra. Emission from the $Br_2(B:v'=11,J'=35)$ state occurred between the $v'=11$ and $v''=4$ vibrational levels. For all the cases in this study, the P-branch emission lines were identified for subsequent measurement. The following table lists the corresponding wavelengths in Angstroms corresponding the $P(J_e)$ and $R(J_e)$ lines identified. These wavelengths are corrected for the index of refraction for air.

Table IX. Line positions for P-R emissions identified by wavelength (Angstroms) and corrected for air.

J	P(J)	R(J)
15	5846.53	5845.42
16	5846.88	5845.69
17	5847.24	5845.98
18	5847.62	5846.29
19	5848.02	5846.62
20	5848.45	5846.97
21	5848.89	5847.34
22	5849.35	5847.73
23	5849.83	5848.14
24	5850.32	5848.56
25	5850.84	5849.01
26	5851.38	5849.48
27	5851.94	5849.96
28	5852.51	5850.46
29	5853.11	5850.99
30	5853.72	5851.53
31	5854.36	5852.09
32	5855.01	5852.67
33	5855.69	5853.28
34	5856.38	5853.90
35	5857.09	5854.54
36	5857.83	5855.20

37	5858.58	5855.87
38	5859.35	5856.57
39	5860.14	5857.29
40	5860.95	5858.03
41	5861.78	5858.79
42	5862.63	5859.56
43	5863.50	5860.36
44	5864.39	5861.17
45	5865.30	5862.01
46	5866.23	5862.86
47	5867.18	5863.74
48	5868.15	5864.63
49	5869.14	5865.55
50	5870.14	5866.48

Appendix B - Error Analysis

As noted in the various tables and graphs of this study, the estimated error limit for convolved and deconvolved rates was +/- 30%. This error bound was derived from the associated uncertainties in measuring emission line peak heights and the propagation of this error through to calculation of the reported rates. Further discussion of sources of error is merited.

Systematic errors associated with conduct of Perram's experiment are drawn from his PhD Dissertation. Pressure changes during spectral runs were always less than 2 % and generally less than 0.02%. The average pressure from beginning to end of each spectral run was used for calculations in this study.

Variations in excitation laser power and small changes in laser frequency generate significant errors in resolved emission spectra intensities. These fluctuations were corrected for by scaling all emission lines observed to a specific value for observed total unresolved fluorescence. This correction is explained in section 2.3.1 and highlighted in Figure 8.

Mathematical corrections were made to emission line intensities to compensate for variations in the relative spectral response of the detection system over the frequency range examined. Spectral response calibration curves are shown in Figure 7 and details of this correction are explained in section 2.3.1.

The total error associated with variations in pressure, excitation laser intensity and detection system spectral response is estimated to be < 5%.

The primary source of error arises from the physical measurement of the specific resolved emission lines used to generate population ratios. Peak heights of individual lines were measured from a "floating" baseline in order to compensate for signal noise in the emission spectra. This floating baseline varied from emission peak to peak. For wider emission lines, the floating baseline varied from the left to the right side of the emission line. An average value centered under the peak of the emission line was used. An uncertainty of half the difference of the baseline measured on the left side of the peak versus the right side of the peak was generated. Additionally, for numerous emission lines, the precise location of the "peak" left a small uncertainty. The combination of these two values represented the total uncertainty associated to a specific peak height measurement. An uncertainty for each population ratio, N(J)/N(Jo), was derived using standard propagation of error statistical methods as described in P. R. Bevington's manuscript on "Data Reduction and Error Analysis". (2:62) Population error bounds based on peak height measurement uncertainties ranged from 5 to 25 % with a typical value of 15%. Propagation of this error through the Stern-Volmer analysis methods discussed increased these errors to a typical value of 25%. Mathematical error bounds related to these uncertainties are noted for total rotational removal rates listed in Tables III and IV.

A nonlinear least-squares fitting program was used to derive nonlinear fits to the data for calculation of both convolved rates and deconvolved rates. The error associated with these fits were generally less than 5%.

Easily, the primary source of in these calculations was attributed to the measurement of peak height values used in population determinations. Error contributions from other sources

were generally negligible compared to this value. The upper estimated error limit for convolved and deconvolved rates incorporating all these variables was 30%

One error source not incorporated into these statistics was the "anomaly" described in detail earlier. The source and magnitude of this effect is unknown. This anomaly effected convolved rates for $21 < J_f < 25$ for rotational transfer out of the (11,35) state. Since these rates were used in the deconvolution process, this unknown error was in turn propagated into the deconvolved rates.

Bibliography

1. Barrow, R. F., Et Al, "The B-X System of Br2: Rotational Analysis, Franck-Condon Factors, and Long Range Potential", *Journal of Molecular Spectroscopy, 51*, (1974).

2. Bevington, Philip R. *Data Reduction and Error Analysis for the Physical Sciences*, New York: McGraw-Hill, 1969.

3. Clyne, M. A. And M. C. Heaven, "Kinetics of Excited States of Br2 Using Laser Excitation", *J Chem Soc Faraday II, 74*, (1978).

4. Clyne, M. A., M. C. Heaven and S. J. Davis, "Laser Excitation Studies of Br2", *J Chem Soc Faraday II, 76*, (1980).

5. Clyne, M. A. And M. C. Heaven, "Kinetics of Excited States of Br2 Using Laser Excitation", Paper 8/947, The University Press, Aberdeen, Great Britain, (1978).

6. Coxon, J. A., *Molecular Spectroscopy*, London: The Chemical Society, 1972.

7. Davis, S.J., *Gas Flow in Chemical Lasers*, edited by S. Rosenwaks, Berlin; Springer-Verlag, 1987.

8. Davis, S. J. And K. W. Holtzclaw, "Rotational Energy Transfer in Excited States of Halogen Molecules: Transfer from v'=6, J'=72 in IF", *Journal of Chemical Physics, 42*, (1990).

9. Demtroder, Wolfgang, *Laser Spectroscopy: Basic concepts and Instrumentation*, New York: Springer-Verlag, 1988.

10. Harris, D. C. And M. D. Bertolucci, *Symmetry and Spectroscopy: An Introduction to Vibrational and Electronic Spectroscopy*, New York: Dover, 1989.

11. Heaven, M. C. And L. J. Van de Burgt, "Rate Constants For Collisional Deactivation of Br2 by Br2 and He", *Chemical Physics, 103*, (1986).

12. Herzberg, Gerard, *Molecular Spectra and Molecular Structure*, New York: Litton Educational Publishing, 1950.

13. Hyan, G. W. And J. D Baldeschwieder, *Journal of Chemical* Physics, 67, (1962).

14. Jordan, P. C., *Chemical Kinetics and Transport*, New York: Plenum Press, 1980.

15. McCurdy, C. W. And W. H. Miller, "Interference Effects in Rotational State Distributions: Propensity and Inverse Propensity", *Journal of Chemical Physics, 67*, (1977).

16. Perram, G. P., "Visible Chemical Lasers", Proceedings from the International Conference on LASERS '89, (Preprint), (1989).

17. Perram, G. P. And S. J. Davis, "Collision Dynamics of BrCl $B^3\Pi(O^+)$ State", *Journal of Chemical Physics, 84*, (1986).

18. Perram, G. P., "Quenching and Rotational Transfer in Molecular Bromine: Thesis Problem Statement and Background Information", AFIT/ENP, (Unpublished), 1989.

19. Perram, G. P., "Collisional Dynamics of the B-State of Bromine Monochloride", Air force Institute of Technology PhD Dissertation 86-1, 1986.

20. Perram, G. P., "Spectroscopic and Kinetic Studies of a Dye Pumped Br2 (B->X) Laser", Proceedings of the International Conference on LASERS '84, November 1984.

21. Steinfeld, J., *Molecules and Radiation: An Introduction To Modern Molecular Spectroscopy*, Cambridge: MIT Press, 1985.

22. Steinfeld, J. And W. Klemperer, "Energy Transfer Processes in Monochromatically Excited Iodine Molecules", *Journal of Chemical Physics, 42*, (1965).

23. Wodarczyk and Schlossberg, "An Optically Pumped Molecular Bromine Laser", *Journal of Chemical Physics, 67*, (1977).

24. Yamasaki and Leone, "Quenching and Energy Transfer Processes of Single Rotational Levels of Br2", *Journal of Chemical Physics, 90*, (1989).

25. Pritchard, D. Et Al, "Power Law Scaling For Rotational Energy Transfer", *Journal of Chemical Physics, 70*, (1979).

26. Yardley, James T, *Introduction To Molecular Energy Transfer*, Morristown, New Jersey: Academic Press, 1980.

27. Brunner, Timothy A et Al, "Rotational Energy Transfer in Na_2 ($1^1\Sigma$) Colliding with Xe, Kr, Ar, Ne, He, H_2, CH_4, and N_2: Experiment and Fitting Laws", *Journal of Chemical Physics*, 74(6), (1981).